INL/EXT-18-51367

MP-1 Intermediate Characterization Report Summary

Fidelma Giulia Di Lemma,
Tammy Trowbridge, Chad Brizzee,
and Jan-Fong Jue

September 2018

The INL is a U.S. Department of Energy National Laboratory
operated by Battelle Energy Alliance

INL/EXT-18-51367

MP-1 Intermediate Characterization Report Summary

**Fidelma Giulia Di Lemma,
Tammy Trowbridge, Chad Brizzee,
and Jan-Fong Jue**

September 2018

**Idaho National Laboratory
Idaho Falls, Idaho 83415**

http://www.inl.gov

**Prepared for the
U.S. Department of Energy
National Nuclear Security Administration
Under DOE Idaho Operations Office
Contract DE-AC07-05ID14517**

MP-1 Intermediate Characterization Report Summary

INL/EXT-18-51367
Revision 0

September 2018

Approved by:

Tammy Crowbridge — 9/13/2018
Name — Date
USHPRR Program Peer Reviewer/Author

[signature] — 9/13/2018
Name — Date
Post Irradiation Examinations Manager

Tammy Crowbridge for Bruce Nielson per email — 9/13/2018
Name — Date
M3 Fuel Fabrication Manager

SUMMARY

The current MP-1 FFC campaign was devised as a verification study of characterization techniques in an effort to standardize methods and measurements for U-Mo fuel plate characterization. This study was conducted in parallel in between four independent laboratories (INL, PNNL, LANL, and BWXT) and utilizing similar equipment. Fuel plates characterized in this effort varied in fabrication parameters including casting methods, rolling schedules and methods, and homogenization treatments. Indexed sections from the fabricated plates were sent to each of the four laboratories to determine Mo distribution, grain size, density, hardness, precipitate size and distribution and gamma phase decomposition. The focus of this work is to attempt to understand of the impact of processing conditions on the final fuel microstructure produced utilizing processes that are commercially feasible requirements. This report summarizes the data collected and analyzed at INL at the one year mark into this two year campaign.

CONTENTS

FIGURES

TABLES

ACRONYMS

ATR	Advanced Test Reactor
BWXT	Babcock and Wilcox Technologies
DOE	Department of Energy
EDX	elemental dispersion x-ray
HEU	highly enriched uranium
INL	Idaho National Laboratory
LABE	low-angle backscattered electron
LANL	Los Alamos National Laboratory
LEI	lower secondary electron detector
LEU	low-enriched uranium
NNSA	National Nuclear Security Administration
OM	optical microscopy
PNNL	Pacific Northwest National Laboratory
SEM	scanning electron microscopy
USHPRR	United States High-Performance Research Reactor
WDS	wave dispersive spectroscopy

MP-1 Intermediate Characterization Report Summary

1. INTRODUCTION

Great effort worldwide has been invested in replacing highly enriched uranium (HEU) fuel with low-enriched uranium (LEU) fuel in nuclear plants. This effort aims in safeguarding nuclear material and promoting the proliferation resistance of current reactors. The United States Department of Energy (DOE), National Nuclear Security Administration's (NNSA) Materials Management and Minimization Reactor Conversion program is actively working to convert civilian research and test reactors from the use of HEU to LEU fuel. To date, DOE NNSA has converted or verified the shutdown of various domestic reactors and also reactors worldwide. The task to develop and test a new LEU fuel while maintaining current performances has been assigned to the United States High-Performance Research Reactor (USHPRR) program. U alloyed with Mo achieves the goal of high uranium density necessary for the conversion of the high performance research reactors, and has also demonstrated good performance in pile [1]. The alloying process of U with Mo stabilizes the body-centered cubic (bcc) gamma phase (γ-U) at room temperature. Without this enhancement to alloying properties, this phase is only stable at temperatures only above 770°C. Retaining this isotropic gamma phase within the U-Mo alloy provides swelling and oxidation resistance and desired mechanical properties [2]. Generally 10% w. has been considered sufficient to achieve stabilization. However, local phenomena within the alloy can affect the local Mo content and lead to gamma phase decomposition. Because of this, it has been suggested that controlling gamma phase decomposition is most critical during processing [2,3]. The work detailed in this document is part of the USHPRR program and focuses on the characterization of fresh fuel (a.k.a., as-fabricated, before-reactor testing) in collaboration with other laboratories including Pacific Northwest National Laboratory (PNNL), Los Alamos National Laboratory (LANL) and Babcock and Wilcox Technologies (BWXT). This testing is part of a four-way validation for which similar samples from master plates were taken and distributed to each laboratory to independently analyze utilizing a standardized set of measurement and analysis procedures. When complete, this work will supply a toolbox of information for alloying and fabrication parameters with their direct effects on microstructure quantified. Various parameters have been analyzed in this characterization effort (including grain size, quality of the barrier layer, alloy composition of the samples, carbide content) based on the direction of the working group in Reference [4]. The final aim of this work is to increase the understanding of the impact of processing conditions on the final fuel microstructure using fabrication processes that meet commercial-viability requirements [4]. The strength of this campaign rests on the extent of the samples studied and the variation of the manufacture parameters; these will permit the program to achieve required understanding, thus permitting the use of these experiments in down-selecting test samples to evaluate irradiation performance [4] and to be tested in various locations within the Idaho National Laboratory's (INL's) Advanced Test Reactor (ATR).

2. INSTRUMENTS

2.1 Samples and their Preparation

The samples analyzed were U-10Mo foils produced by BWXT. These included as-cast plates, cold and hot rolled plates, and also plates which included a Zr coating layer. The Zr coating is obtained by co-rolling Zr foil together with the alloyed fuel stock. The Zr is added as a diffusion-barrier layer between the fuel foil and the Al cladding, a process typically used in fabrication of this fuel type in order to avoid the formation of an interaction layer in between the U-Mo fuel and the Al cladding, which can to lead to cladding failure during irradiation [5]. These samples were received by INL to perform extensive characterization, as is described in the following sections.

The samples received were prepared for following analyses as prescribed in Reference [4]. U-10Mo foils were cut, mounted, and polished. From each foil, six samples were obtained as follows: subsamples were cut using a low-speed saw (Buehler Isomet) from the forward edge (indicated in our report as Met 1-F), from the middle section (Met 2-M), and finally from the back edge (Met 3-B). For each section, a longitudinal cut and transverse cut were performed (hereafter, Longi, and Trans, respectively). An example of a cutting diagram from Reference [4] is shown in Figure 1. After sectioning, the samples were sandwiched between glass slides and embedded in epoxy resin (Buehler Epoxy Thin 2) for grinding and polishing. Grinding and polishing was performed as directed in Reference [4], and summarized in Table 1. However, due to the limitation of the facility, plasma cleaning could not be performed.

Following preparation by polishing, the samples were left for at least 3 days in air storage for oxidation promoting the visualization of the grain structure for the further-required optical microscopy (OM) analysis, as described in References [4 and 5]. These analyses were performed to determine grain size and to evaluate important defects and gamma phase decomposition. The full length of the samples were analyzed, and images were collected to obtain complete full-section montages of the optical images.

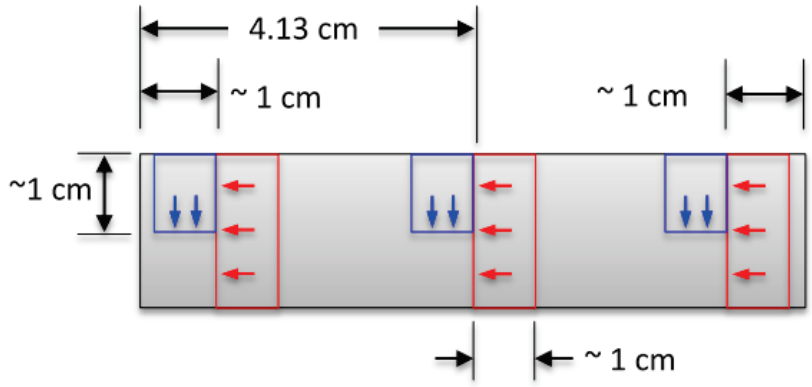

Figure 1. Example of cutting diagram for a foil from Reference [4].

Table 1. Grinding and polishing applied for sample preparation.

Step	Grid	Time	System used
1	180	Until Planar on back side	Buehler Ecomet 250 Autopolisher
2	240	1 minute	
3	400	1 minute	
4	600	2 minutes	
5	1200	2 minutes	
6	9µm diamond suspension	1 minute	
7	3µm diamond suspension	1 minute	
8	1µm diamond suspension + lapping oil	24 hours	Buehler Vibromet 2 Vibropolisher
9	50/50 0.08 µm colloidal SiO_2 + deionized water	24 hours	
10	1% acetic acid + deionized water	1 minute	Hand polished + ethanol cleaned

After optical microscopy, samples were coated for further scanning electron microscopy (SEM) analyses, coupled with elemental dispersion x-ray analyses (EDX). The samples were coated using the Hummer 6.2 sputtering system, using a gold target. Factory recommended settings for the machine were employed, applying a 90–100 s sputtering at 15 mA in argon for each sample. These parameters correspond to a nominal Au-coating thickness in between 5–6 nm. However, due to unstable vacuum conditions influencing deposition rates, some variation in the coating thickness is observed by variation of Au w%. by EDX analyses. Coating with these parameters was deemed successful due to non-charging samples. Au was identified and confirmed by EDX, which minimally influenced the analyses and was generally under the limit of the working-group practice (5 wt.%). Samples in red in Table 2 indicate the samples analysis for which the gold layer yielded a content higher than 5% wt.

A list of the samples, together with a summary of the main results obtained are reported in Table 2. Blank spaces found in the table indicate the analyses are currently in progress, while "N.A." (i.e., not available) indicates that the particular parameter analyzed does not apply to that sample, or the phenomena was not observed. Finally "Y" indicates that the analysis has been completed or the phenomena was observed.

Table 2. List of samples, analyses performed, and summary of the main results.

			Optical		SEM/EDX				
No.	Sample Name	Cut	Grains d (μm)	Montage	Thickness (μm)	Zr Thickness (μm)	Carbides V*i* (%)	Mo distribution ($\%_{wt.}$)	γ phase dec.
Decan Samples Casted									
1	028-01-000DTA	Met1-FLongi	31.8-44.9	Y	1344	N.A.	0.48	9.68-10.34	Y
2		Met1-FTrans	37.8-53.4	Y	1407	N.A.	0.45	9.73-10.2	Y
3		Met2-MLongi	31.8-44.9	Y	1481	N.A.	1.01	9.10-10.11	Y
4		Met2-MTrans	22.5-37.8	Y	1487	N.A.	0.86	9.15-10.21	Y
5		Met3-BLongi	22.5-31.8	Y	1409	N.A.	0.66	9.55-9.99	Y
6		Met3-BTrans	44.9-53.4	Y	1326	N.A.	0.57	9.31-10.41	Y
7	028-01-002DTB	Met1-FLongi	26.7-31.8	Y	1471	N.A.	0.69	9.76-10.22	Y
8		Met1-FTrans	26.7-31.8	Y	1485	N.A.	0.58	9.59-10.06	Y
9		Met2-MLongi	31.8-44.9	Y	1431	N.A.	0.49	9.55-9.95	Y
10		Met2-MTrans	26.7-37.8	Y	1439	N.A.	0.55	9.43-10.00	Y
11		Met3-BLongi	26.7-37.8	Y	1535	N.A.	0.56	10.13-10.98	Y
12		Met3-BTrans	22.5-31.8	Y	1562	N.A.	0.46	9.65-10.05	Y
13	028-01-000DTC	Met1-FLongi	22.5-31.8	Y	1441	N.A.	0.52	9.51-10.26	Y
14		Met1-FTrans[a]	26.7-31.8		1433	N.A.	0.49	9.52-10.54	Y
15		Met2-MLongi	26.7-31.8	Y	1468	N.A.	0.54	9.62-10.11	N.A.
16		Met2-MTrans	26.7-37.8		1476	N.A.	0.48	9.62-10.17	Y
17		Met3-BLongi	26.7-31.8	Y	1475	N.A.	0.57	9.72-10.13	Y
18		Met3-BTrans	26.7-31.8	Y	1491	N.A.	0.52	9.78-10.25	Y
19	028-05-000DTA	Met1-FLongi	26.7-37.8	Y	1614	N.A.	1.21	9.78-10.82	Y
20		Met1-FTrans	22.5-37.8	Y	1607	N.A.	1.36	9.85-11.49	Y
21		Met2-MLongi	26.7-31.8	Y	1635	N.A.	0.57	9.87-10.80	N.A.
22		Met2-Trans	26.7-37.8	Y	1658	N.A	0.16	10.55-11.17	N.A.
23		Met3-BLongi	22.5-31.8	Y	1423	N.A.	0.65	10.10-11.04	Y
24		Met3-BTrans	22.5-31.8	Y	1548	N.A.	1.04	10.11-10.96	Y
25		Met1-FLongi	31.8-37.8	Y	1537	N.A.	0.82	10.00-10.91	Y

a. This sample was very small (ca. 1.9*1.5 mm) due to sample preparation, as the complete sample was not retrievable by polishing from the epoxy, due to incorrect mounting. Due to the small area analyzed statistical significance may be lost on the result provided due to the limited area analyzed.

No.	Sample Name	Cut	Optical		SEM/EDX				
			Grains d (µm)	Montage	Thickness (µm)	Zr Thickness (µm)	Carbides Vi (%)	Mo distribution ($\%_{wt.}$)	γ phase dec.
26	028-05-002DTB	Met1-FTrans	26.7-37.8	Y	1482	N.A.	0.81	10.19-10.82	N.A.
27		Met2-MLongi	26.7-37.8		1512	N.A.	0.65	9.59-10.04	Y
28		Met2-MTrans	26.7-31.8		1514	N.A.	0.71	9.61-10.00	Y
29		Met3-BLongi	22.5-31.8	Y	1438	N.A.	0.63	10.03-10.69	Y
30		Met3-BTrans	22.5-31.8	Y	1451	N.A.	0.80	10.08-10.98	Y
31	028-05-000DTC	Met1-FLongi	26.7-31.8	Y	1481	N.A.	0.90	9.63-10.13	N.A.
32		Met1-FTrans	31.8-37.8		1462	N.A.	1.05	9.38-9.88	Y
33		Met2-MLongi	26.7-37.8	Y	1443	N.A.	0.87	9.91-10.38	Y
34		Met2-MTrans	37.8-44.9	Y	1433	N.A.	0.78	9.51-10.19	Y
35		Met3-BLongi	22.5-26.7	Y	1495	N.A.	0.99	9.39-9.78	Y
36		Met3-BTrans	26.7-31.8	Y	1486	N.A.	0.59	9.45-9.93	Y
Cold Rolled/Annealed Samples									
37	027-05-002CTA	Met1-FLongi	18.9-22.5		690	N.A.	1.46	9.62-10.47	Y
38		Met1-FTrans	18.9-26.7		689	N.A.	1.47	9.51-10.28	Y
39		Met2-MLongi	18.9-22.5	Y	722	N.A.	1.77	9.54-10.43	Y
40		Met2-MTrans	18.9-26.7	Y	724	N.A.	1.35	9.34-10.24	Y
41		Met3-BLongi	22.5-26.7	Y	623	N.A.	1.31	9.70-10.20	Y
42		Met3-BTrans	18.9-26.7	Y	633	N.A.	1.59	9.76-10.30	Y
43	027-05-002CTB	Met1-FLongi	26.7-31.8		684	N.A.	1.83	9.72-10.20	Y
44		Met1-FTrans	26.7-31.8		681	N.A.	1.69	9.42-9.89	Y
45		Met2-MLongi	26.7-31.8		709	N.A.	1.36	9.38-9.90	N.A.
46		Met2-MTrans	22.5-31.8		710	N.A.	1.46	9.53-10.25	Y
47		Met3-BLongi	22.5-31.8		698	N.A.	1.60	9.32-9.77	Y
48		Met3-BTrans	22.5-31.8		705	N.A.	1.55	9.40-10.10	Y
49	027-05-002CTC	Met1-FLongi	18.9-26.7		718	N.A.	1.80	9.68-10.35	Y
50		Met1-FTrans	15.9-22.5	Y	729	N.A.	1.74	9.44-10.42	Y
51		Met2-MLongi	18.9-26.7	Y	755	N.A.	1.83	9.64-10.13	Y
52		Met2-MTrans	18.9-26.7	Y	754	N.A.	1.59	9.61-11.33	Y
53		Met3-BLongi	15.9-22.5		724	N.A.	1.72	9.66-10.37	Y
54		Met3-BTrans	15.9-22.5		737	N.A.	1.45	9.63-10.45	Y
55	028-05-001CTA	Met1-FLongi	18.9-26.7		713	N.A.	1.02	9.58-11.14	Y
56		Met1-FTrans	18.9-26.7		691	N.A.	1.10	10.27-10.92	Y
57		Met2-MLongi	22.5-26.7		726	N.A.	0.89	10.10-10.97	Y
58		Met3-BLongi	22.5-26.7		722	N.A.	1.06	10.16-10.98	Y
59		Met2-MLongi	18.9-26.7		713	N.A.	0.69	10.34-11.18	Y
60		Met3-BTrans	18.9-22.5		715	N.A.	0.80	9.57-10.34	Y
61	028-05-001CTB	Met1-FLongi	18.9-26.7		710	N.A.	0.80	9.36-10.21	Y
62		Met1-FTrans	18.9-26.7		698	N.A.	0.90	9.60-10.06	Y
63		Met2-MLongi	18.9-26.7		725	N.A.	0.84	9.66-10.97	Y
64		Met2-MTrans	22.5-31.8		728	N.A.	0.77	9.61-10.21	N.A.
65		Met3-BLongi	18.9-26.7		725	N.A.	0.78	9.30-10.15	Y
66		Met3-BTrans	22.5-26.7		729	N.A.	0.77	9.34-9.93	Y
Decan Samples Casted with Zr									
67		Met1-FLongi	31.8-44.9		1449	56	0.93	9.56-10.39	Y

No.	Sample Name	Cut	Optical		SEM/EDX				
			Grains d (µm)	Montage	Thickness (µm)	Zr Thickness (µm)	Carbides Vi (%)	Mo distribution ($\%_{wt.}$)	γ phase dec.
68	029-05-000DTA	Met1-FTrans	31.8-44.9		1446	53	0.64	9.39-9.83	Y
69		Met2-MLongi	37.8-53.4		1480	57	0.83	8.93-10.07	Y
70		Met2-MTrans	37.8-53.4		1438	57	0.85	10.36-11.10	Y
71		Met3-BLongi	31.8-44.9		1413	59	0.81	9.38-10.48	Y
72		Met3-BTrans	37.8-44.9		1375	61	0.8	9.36-10.38	Y
73	029-05-002DTB	Met1-FLongi	44.9-53.4		1507	62	1.00	9.55-10.20	Y
74		Met1-FTrans	44.9-53.4		1447	60	0.82	9.66-10.34	Y
75		Met2-MLongi	44.9-63.5		1495	57	0.91	10.59-11.51	Y
76		Met2-MTrans	53.4-63.5		1543	55	0.64	10.28-10.97	Y
77		Met3-BLongi	53.4-63.5		1476	64	0.90	9.48-10.04	Y
78		Met3-BTrans	53.4-75.5		1518	53	0.89	9.50-10.31	Y
79	029-05-000DTC	Met1-FLongi	37.8-44.9		1446	54	0.72	9.49-9.98	Y
80		Met1-FTrans	37.8-44.9		1432	59	0.65	9.39-9.92	Y
81		Met2-MLongi	26.7-37.8		1606	58	0.70	9.54-9.79	Y
82		Met2-MTrans	37.8-44.9		1606	53	0.72	9.60-10.03	Y
83		Met3-BLongi	26.7-37.8		1572	61	0.74	9.52-9.97	Y
84		Met3-BTrans	26.7-37.8		1589	59	0.62	9.46-9.99	Y
85	030-01-000DTC	Met1-FLongi	44.9-53.4		1448	110	0.68	9.56-10.04	Y
86		Met1-FTrans	44.9-53.4		1497	131	0.68	9.67-10.10	Y
87		Met2-MLongi	44.9-63.5		1554	14	0.70	9.57-10.31	Y
88		Met2-MTrans	44.9-53.4		1530	122	0.76	9.75-10.11	Y
89		Met3-BLongi	37.8-53.4		1607	98	0.69	9.66-10.14	Y
90		Met3-BTrans	44.9-63.5		1569	90	0.71	9.44-10.16	Y
Cold Rolled/Annealed Samples with Zr									
91	029-05-0001CTA	Met1-FLongi	26.7-37.8						
82		Met1-FTrans	31.8-37.8						
83		Met2-MLongi	26.7-37.8						
84		Met2-MTrans	26.7-37.8						
95		Met3-BLongi	26.7-37.8						
96		Met3-BTrans	26.7-31.8						
97	029-05-004CTB	Met1-FLongi	22.5-26.7						
98		Met1-FTrans	22.5-31.8						
99		Met2-MLongi	22.5-31.8						
100		Met2-MTrans	26.7-31.8						
101		Met3-BLongi	26.7-31.8						
102		Met3-BTrans	26.7-37.8						
103	029-05-001CTC	Met1-FLongi	22.5-31.8						
104		Met1-FTrans	22.5-31.8						
105		Met2-MLongi	22.5-31.8						
106		Met2-MTrans	26.7-31.8						
107		Met3-BLongi	26.7-31.8						
108		Met3-BTrans	26.7-37.8						
109	029-05-002CTA	Met1-FLongi	22.5-31.8						
110		Met1-FTrans	18.9-26.7						

No.	Sample Name	Cut	Optical		SEM/EDX				
			Grains d (µm)	Montage	Thickness (µm)	Zr Thickness (µm)	Carbides V*i* (%)	Mo distribution ($\%_{wt.}$)	γ phase dec.
111		Met2-MLongi	22.5-31.8						
112		Met2-MTrans	22.5-31.8						
113		Met3-BLongi	22.5-26.7						
114		Met3-BTrans	22.5-26.7						
115	029-05-006CTB	Met1-FLongi	22.5-31.8						
116		Met1-FTrans	22.5-31.8						
117		Met2-MLongi	22.5-31.8						
118		Met2-MTrans	22.5-31.8						
119		Met3-BLongi	22.5-31.8						
120		Met3-BTrans	26.7-37.8						
121	029-05-002CTC	Met1-FLongi	18.9-26.7						
122		Met1-FTrans	22.5-31.8						
123		Met2-MLongi	22.5-31.8						
124		Met2-MTrans	18.9-26.7						
125		Met3-BLongi	22.5-31.8						
126		Met3-BTrans	26.7-37.8						
127	030-01-003CTA	Met1-FLongi	13.3-18.9						
128		Met1-FTrans	13.3-18.9						
129		Met2-MLongi	13.3-18.9						
130		Met2-MTrans	13.3-18.9						
131		Met3-BLongi	15.9-22.5						
132		Met3-BTrans	13.3-18.9						
133	030-01-008CTB	Met1-FLongi	15.9-22.5						
134		Met1-FTrans	18.9-26.7						
135		Met2-MLongi	18.9-22.5						
136		Met2-MTrans	15.9-22.5						
137		Met3-BLongi	18.9-26.7						
138		Met3-BTrans	18.9-26.7						
139	030-01-003CTC	Met1-FLongi	15.9-22.5						
140		Met1-FTrans	22.5-26.7						
141		Met2-MLongi	15.9-22.5						
142		Met2-MTrans	15.9-22.5						
143		Met3-BLongi	18.9-26.7						
144		Met3-BTrans	18.9-26.7						

2.2 Optical Microscope

Samples were analyzed by optical microscopy, using the Zeiss Axio Pro 10 mm. Calibration of the optical microscope is performed every 12 months by the manufacturer's field service engineer during the preventive maintenance with results reported within the instrumentation tolerance in Reference [4]. Furthermore calibration was checked regularly using a NIST approved stage micrometer (2 mm) at all magnifications of interest. Images were collected with different objectives, as requested in Reference [4], and following the procedure of the working group described in detailed in Reference [5]. Images were collected in the bright field mode for the 2.5, 5, 10× objective and in the polarized mode for 10, 20×. Areas of interest were also observed with the 50× objective when possible. Montages were performed for

the samples at 2.5, 5, 10× and/or 20×, as the full length of the samples were analyzed. The performed montages were obtained from the OM images stitched using Photoshop CC2017 [6]; an example at 10× is shown in Figure 2. For higher magnification (20, 50×) characteristic images were recorded in the center, left and right regions. The Photoshop software was also used to enhance images to obtain the best contrast for grain-size determination. These analyses were performed as required in Reference [4], and following the standard procedure in Reference [7]. Their results are further described in the results section.

Figure 2. Example of a montage performed for the foil 028-05-000DTA middle section transversal cut (MET2-MTrans). This plate show large carbide deposits in the central region and some deformation, probably related to sample preparation, leading to a corrugated profile.

2.3 Scanning Electron Microscope

Following optical microscopy, the samples were analyzed with the JEOL 7600-F (Field emission gun) at 20 KeV, in HC14. The aperture used was 110 mm, as prescribed in References [4 and 5]. These settings corresponded to a current of ~4.7 nA. Images were taken with the low-angle backscattered electron (LABE) detector at high contrast and with the lower secondary electron detector (LEI), 30 s per frame with five frames averaged. Preventive maintenance and magnification compliance of this instrument is performed two times per year by the manufacturer's field service engineer, and it is in compliance with the requirement in Reference [4]. Images across the entire length of the samples were acquired at 45-50 X in LEI mode to create montages using Photoshop CC2017 software [6]. An example is presented in Figure 3. Interesting microstructural features, such as carbides, oxide skins, gamma-phase decomposition etc., were recorded at magnifications prescribed by the test plan (250, 1000, and 2500×) and collected with both the LEI and LABE detector. Examples of interesting features are shown in Figure 4. Through these images, both the morphology and chemical features of the samples were highlighted. For example, cracks were observed in the forward or back leading edges of the samples, (Figure 4). This is probably due to the sample preparation itself, and it is not inherent to the fuel-foil fabrication. However, in these samples, cracks were also observed in the presence of large oxide-carbide, or oxide skins, (Figure 4), also in the middle of the sample. These cracks may be formed due to the highly brittle character of the carbide phase paired with stresses of sample preparation; thus, presence of carbides should be highly characterized for these fuel samples. Carbide size distribution and its volume fraction for each sample was determined following the procedure reported in References [4, 8, and 9], using images collected with the LABE detector at 250×. The procedure applied and results obtained for these analyses are detailed further in the results section.

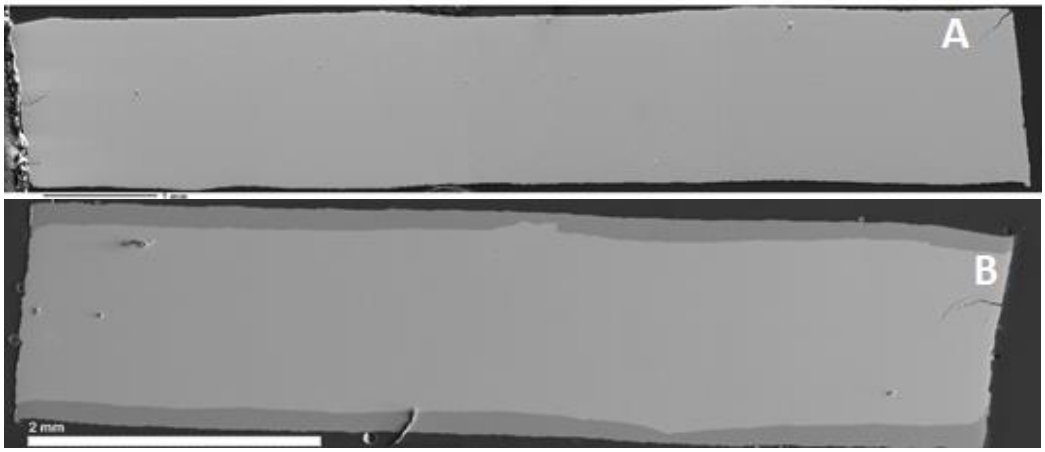

Figure 3. Example of a montage performed for two samples named 028-05-000DTC-MET3-BLongi (A), and Zr coated 030-01-000DTC-MET3-BLongi (B). This plate shows cracks at the edge of the sample and some deformation leading to a corrugate profile.

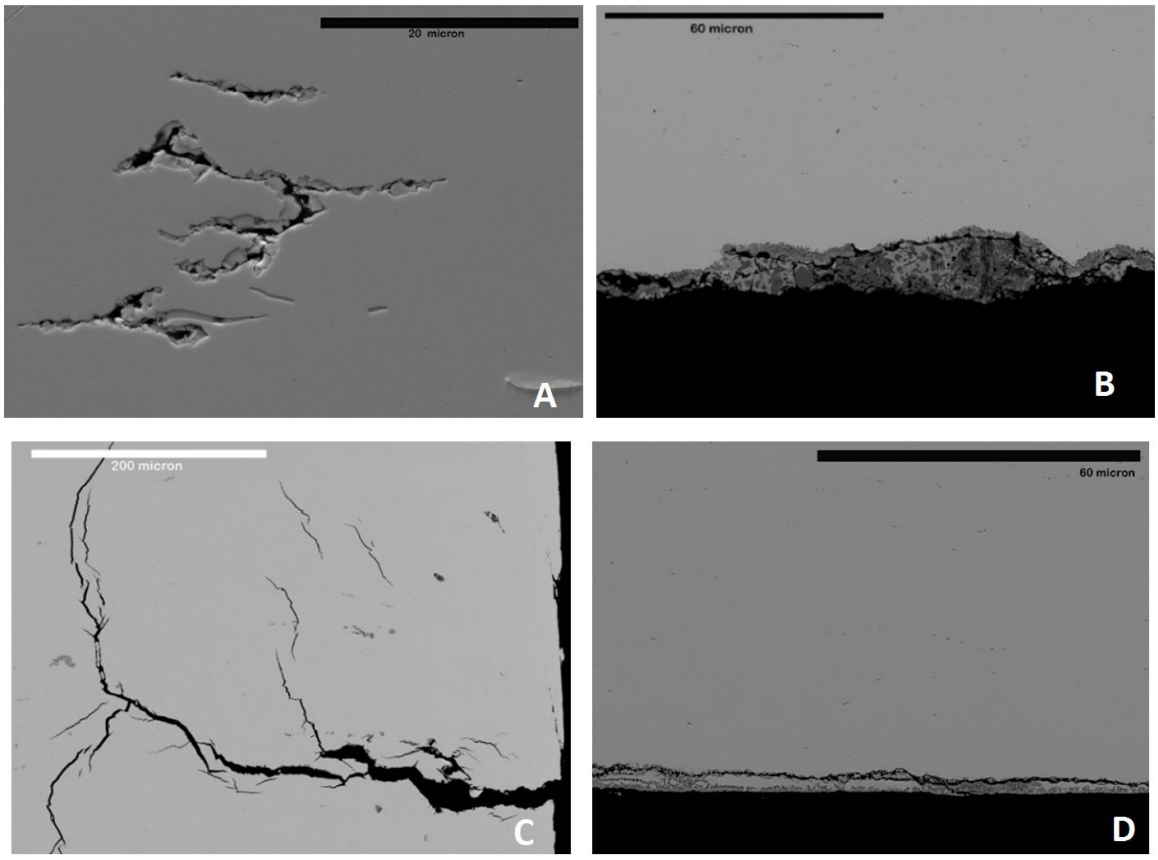

Figure 4. Examples of microstructural features observed: image A (028-05-001CTA-Met2-MTrans) shows the presence of a carbide leading to crack formation in the central part of the fuel meat. An oxi-carbide skin on the fuel meat is observed on Sample 028-01-000DTA-Met3-BLongi (B). The different composition can be observed by the differences in contrast on the LABE detector. (C) Cracks developing from the edge of the sample in the carbide can be seen in image C, for sample 028-01-002DTB-Met3-Longi, and may be related to sample preparation. Image D (028-05-001CTA-Met2-MLongi) shows a long crack (longer than 1 mm), developed from the oxide skin, similar to image B.

Moreover, quantitative EDX analyses were collected at a 15 mm working distance using an Oxford X-max 20 mm^2 detector. EDX analyses were performed using a line scan to evaluate Mo distribution in the sample at a magnification of 1000× and steps of 1 µm across the height of the sample, as directed by Reference [4]. Mo chemical banding was evaluated with this method because it was not visible by imaging in high-contrast LABE. From sample No.79, the working-group procedure has been revised to include at least 100 points in this analyses. This led to the necessity of rotating the sample to have a larger area to obtain the 100 µm length necessary for this line scan. The elemental line scans were performed with an acquisition time of 60 s for each step and process time 2 to maintain the required dead time of over 30%. EDX mapping and point analyses were finally used to evaluate the composition of the carbides and of the interaction layer when the Zr coating was present (from sample No.67). Wavelength dispersive X-ray mapping (with the Oxford Inca Wave) and line scans were also performed on the interaction layer for the Zr-coated samples. During these analyses, the current was increased to HC 17 to obtain relevant counting statistics. A summary of the performed analyzes and parameters applied are further presented in Table 3.

Table 3. Summary of the SEM analyses and parameters applied.

Analyses	Sample type	Magnification	Detector	Current	Time	Frames/Process time (PT)
Imaging	all	45-50×, 250×, 1000×, 2500×	LEI and LABE	HC 14	30 s	5
Precipitates	all	1000×	EDX point	HC 14	30-60 s	PT 2
Chemical banding	all	1000×	EDX line scan	HC 14	30-60 s 1 µm step	PT 2
Precipitates	all	1000×	EDX map	HC 14	Dwell time 100 µs	100
Interaction layer	Zr coated	2500×	WDX line	HC 17	Dwell time 100 µs	500
Interaction layer	Zr coated	2500×	EDX line	HC 14	20 s 0.1 µm step	PT 2
Interaction layer	Zr coated	2500×	WDX/ EDX map	HC 17	Dwell time 100 µs	500

3. RESULTS

This section presents a summary of the obtained results, together with example images of the typical or significant features observed on the samples.

3.1 Grain Size

The images collected by OM were used to determine the grain size, applying the procedure in ASTM E112-113 [7] and using the Heyn Lineal intercept method. Up to 500 mm of straight lines were used to perform the analyses. The images analyzed were acquired with 10 or 20× objective in polarized light, depending on grain resolution and aiming to count ~50 intercepts as prescribed in Reference [7]. The OM images were generally modified by Photoshop CC2017 [6] to obtain higher contrast between grains and facilitate grain visualization (as shown in Figure 5). The images were opened with the Photoshop CC2017 software and modified. The enhanced images were visualized on the computer screen, and the prescribed intercept grid was superimposed for counting. An example of the test-pattern grid used can be found in

Reference [7]. In Table 4, a summary of the grain-size results obtained by this method are presented. The grain-size-diameter variation in Table 4 was obtained based on the standard deviation and from Reference [7], which reports the relationship of grain-size diameter to grain size number for each 0.5 grain-size-number step. For quick comparison, the data are also summarized in Figure 6. In this figure, the data are obtained from the average of the six samples analyzed for each foil. It is worth noticing that some samples did not present a clear grain structure. This may have been related to sample deformation. The questionable datasets are highlighted in red in Table 4. These data generally exhibited a higher standard deviation and lower grain size number, corresponding to larger grain diameters. This is caused by the fact that the deformation bands do not permit the visualization of all the grains, leading to a lowered intercept count, and thus erroneously larger grain diameters.

The analyses by OM have been completed for all samples; from the data, it can be inferred that cast samples present larger grain sizes, 30–40 μm, while the cold-rolled, annealed samples, although annealed present a smaller grain size of 25 μm or smaller. This behavior is also clearly visible in the example micrographs presented Figure 5.

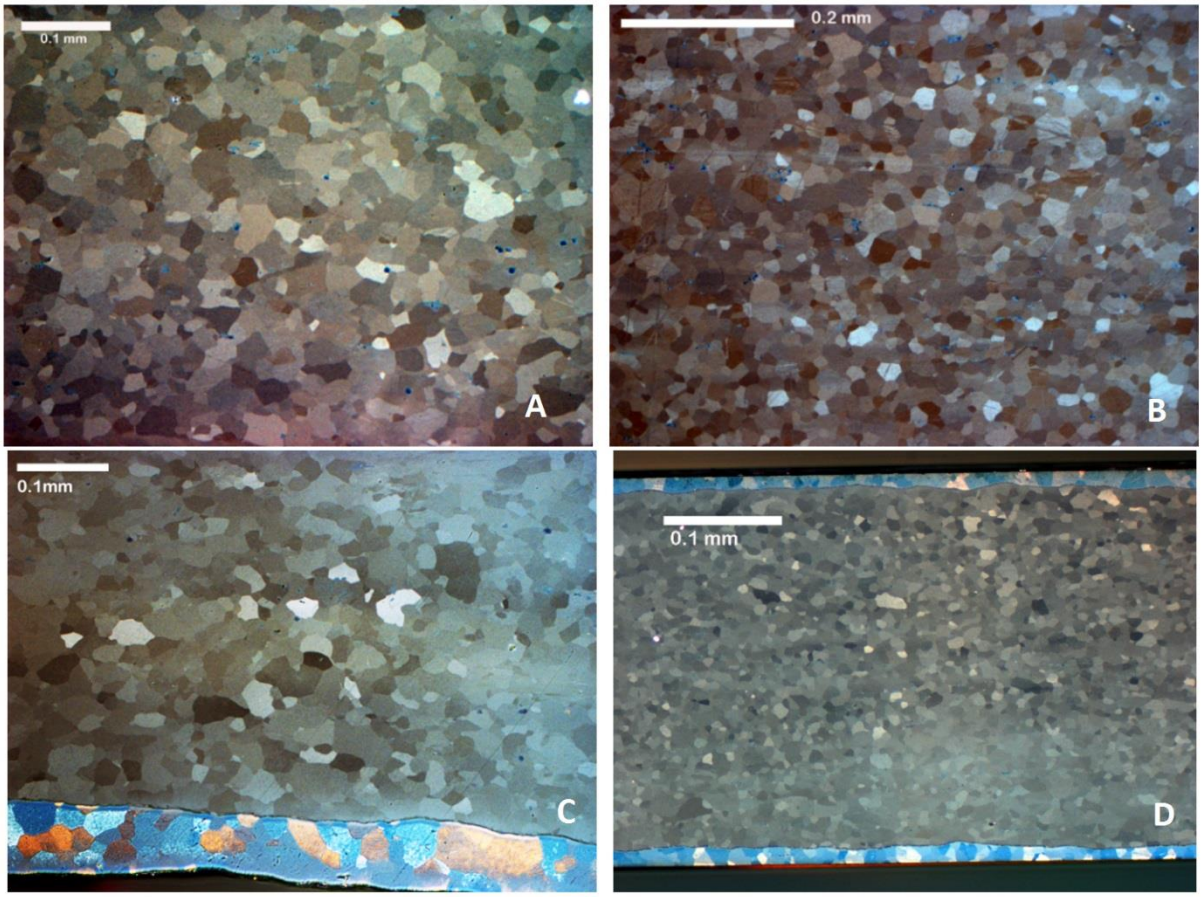

Figure 5. Example of grain structure for the different samples analyzed: Image A, a cast sample (028-01-002DTB-Met1-FTrans); B, a cold-rolled, annealed sample (028-05-001CTA-Met3-BTransi); C, a cast foil with Zr coating (028-05-001CTB-Met2-MLongi); D, a cold-rolled, annealed foil with Zr coating (029-05-001CTA-Met3-BTrans).

Table 4. Grain size numbers and grain diameter obtained by optical analyses. Red values present large variation and/or images in which the grains were poorly visible.

No.	Sample Name	Grain Size No.	Error (Std σ)	Grains d (µm)	No.	Sample Name	Grain Size No.	Error (Std σ)	Grains d (µm)
1	028-01-000DTA	5.99	0.40	37.8-53.4	73	029-05-002DTB	5.84	0.20	44.9-53.4
2		6.65	0.31	31.8-44.9	74		5.82	0.26	44.9-53.4
3		6.80	0.37	22.5-37.8	75		5.59	0.30	44.9-63.5
4		6.64	0.43	31.8-44.9	76		5.23	0.27	53.4-63.5
5		5.87	0.40	44.9-53.4	77		5.22	0.21	53.4-63.5
6		7.54	0.33	22.5-31.8	78		5.06	0.17	53.4-75.5
7	028-01-002DTB	7.28	0.18	26.7-31.8	79	029-05-000DTC	6.25	0.29	37.8-44.9
8		7.22	0.24	26.7-31.8	80		6.22	0.17	37.8-44.9
9		7.07	0.31	26.7-37.8	81		7.04	0.30	26.7-37.8
10		6.78	0.35	31.8-44.9	82		6.23	0.31	37.8-44.9
11		7.30	0.30	22.5-31.8	83		6.91	0.24	26.7-37.8
12		7.08	0.28	26.7-37.8	84		6.87	0.23	26.7-37.8
13	028-01-000DTC	7.36	0.16	26.7-31.8	85	030-01-000DTC	5.74	0.34	44.9-53.4
14		7.43	0.24	22.5-31.8	86		5.88	0.18	44.9-53.4
15		7.11	0.22	26.7-37.8	87		5.61	0.32	44.9-63.5
16		7.23	0.24	26.7-31.8	88		5.88	0.17	44.9-53.4
17		7.20	0.21	26.7-31.8	89		5.85	0.35	37.8-53.4
18		7.13	0.15	26.7-31.8	90		5.71	0.26	44.9-63.5
19	028-05-000DTA	7.24	0.35	22.5-37.8	91	029-05-0001CTA	7.01	0.22	26.7-37.8
20		7.05	0.15	26.7-37.8	82		6.84	0.21	31.8-37.8
21		7.12	0.37	26.7-37.8	83		6.93	0.27	26.7-37.8
22		7.21	0.25	26.7-31.8	84		7.03	0.26	26.7-37.8
23		7.34	0.32	22.5-31.8	95		6.96	0.23	26.7-37.8
24		7.41	0.36	22.5-31.8	96		7.28	0.14	26.7-31.8
25	028-05-002DTB	7.01	0.30	26.7-37.8	97	029-05-004CTB	7.76	0.26	22.5-26.7
26		6.77	0.17	31.8-37.8	98		7.54	0.18	22.5-31.8
27		7.08	0.27	26.7-31.8	99		7.29	0.20	22.5-31.8
28		7.27	0.38	26.7-37.8	100		7.29	0.14	26.7-31.8
29		7.40	0.36	22.5-31.8	101		7.17	0.12	26.7-31.8
30		7.45	0.28	22.5-31.8	102		7.14	0.21	26.7-37.8
31	028-05-000DTC	6.87	0.22	31.8-37.8	103	029-05-001CTC	7.72	0.28	22.5-31.8
32		7.27	0.19	26.7-31.8	104		7.59	0.21	22.5-31.8
33		6.27	0.25	37.8-44.9	105		7.23	0.23	22.5-31.8
34		7.03	0.20	26.7-37.8	106		7.30	0.21	26.7-31.8
35		7.27	0.28	26.7-31.8	107		7.27	0.21	26.7-31.8
36		7.76	0.29	22.5-26.7	108		7.24	0.19	26.7-37.8
37	027-05-002CTA	8.10	0.18	18.9-22.5	109	029-05-002CTA	7.60	0.25	22.5-31.8
38		8.01	0.24	18.9-26.7	110		7.78	0.29	18.9-26.7
39		8.23	0.16	18.9-22.5	111		7.63	0.25	22.5-31.8
40		7.90	0.21	18.9-26.7	112		7.30	0.33	22.5-31.8
41		7.70	0.18	22.5-26.7	113		7.76	0.22	22.5-26.7
42		7.82	0.24	18.9-26.7	114		7.69	0.09	22.5-26.7
43	027-05-002CTB	7.28	0.16	26.7-31.8	115	029-05-006CTB	7.62	0.34	22.5-31.8
44		7.32	0.11	26.7-31.8	116		7.63	0.27	22.5-31.8
45		7.35	0.08	26.7-31.8	117		7.65	0.21	22.5-31.8
46		7.54	0.15	22.5-31.8	118		7.45	0.12	22.5-31.8
47		7.51	0.16	22.5-31.8	119		7.40	0.14	22.5-31.8
48		7.42	0.16	22.5-31.8	120		7.22	0.24	26.7-37.8
49	027-05-002CTC	8.15	0.20	18.9-26.7	121	029-05-002CTC	7.83	0.15	18.9-26.7
50		8.27	0.25	15.9-22.5	122		7.57	0.11	22.5-31.8
51		7.97	0.17	18.9-26.7	123		7.51	0.21	22.5-31.8
52		8.07	0.37	18.9-26.7	124		7.85	0.22	18.9-26.7
53		8.59	0.20	15.9-22.5	125		7.32	0.22	22.5-31.8
54		8.48	0.30	15.9-22.5	126		7.37	0.27	26.7-37.8
55	028-05-001CTA	7.96	0.14	18.9-26.7	127	030-01-003CTA	9.31	0.16	13.3-18.9
56		8.09	0.12	18.9-26.7	128		9.16	0.22	13.3-18.9
57		7.73	0.14	22.5-26.7	129		8.97	0.09	13.3-18.9
58		7.74	0.13	22.5-26.7	130		9.06	0.17	13.3-18.9
59		7.83	0.27	18.9-26.7	131		8.64	0.27	15.9-22.5
60		7.88	0.11	18.9-22.5	132		9.16	0.26	13.3-18.9

No.	Sample Name	Grain Size No.	Error (Std σ)	Grains d (μm)	No.	Sample Name	Grain Size No.	Error (Std σ)	Grains d (μm)
61	028-05-001CTB	7.97	0.13	18.9-26.7	133	030-01-008CTB	8.55	0.26	15.9-22.5
62		8.08	0.18	18.9-26.7	134		8.20	0.25	18.9-26.7
63		7.97	0.16	18.9-26.7	135		8.32	0.15	18.9-22.5
64		7.61	0.20	22.5-31.8	136		8.49	0.21	15.9-22.5
65		7.91	0.22	18.9-26.7	137		8.33	0.12	18.9-26.7
66		7.72	0.18	22.5-26.7	138		8.12	0.19	18.9-26.7
67	029-05-000DTA	6.52	0.26	31.8-44.9	139	030-01-003CTC	8.44	0.21	15.9-22.5
68		6.33	0.25	31.8-44.9	140		7.81	0.15	22.5-26.7
69		6.02	0.27	37.8-53.4	141		8.52	0.11	15.9-22.5
70		5.92	0.21	37.8-53.4	142		8.34	0.20	15.9-22.5
71		6.63	0.31	31.8-44.9	143		8.10	0.19	18.9-26.7
72		6.26	0.14	37.8-44.9	144		8.13	0.20	18.9-26.7

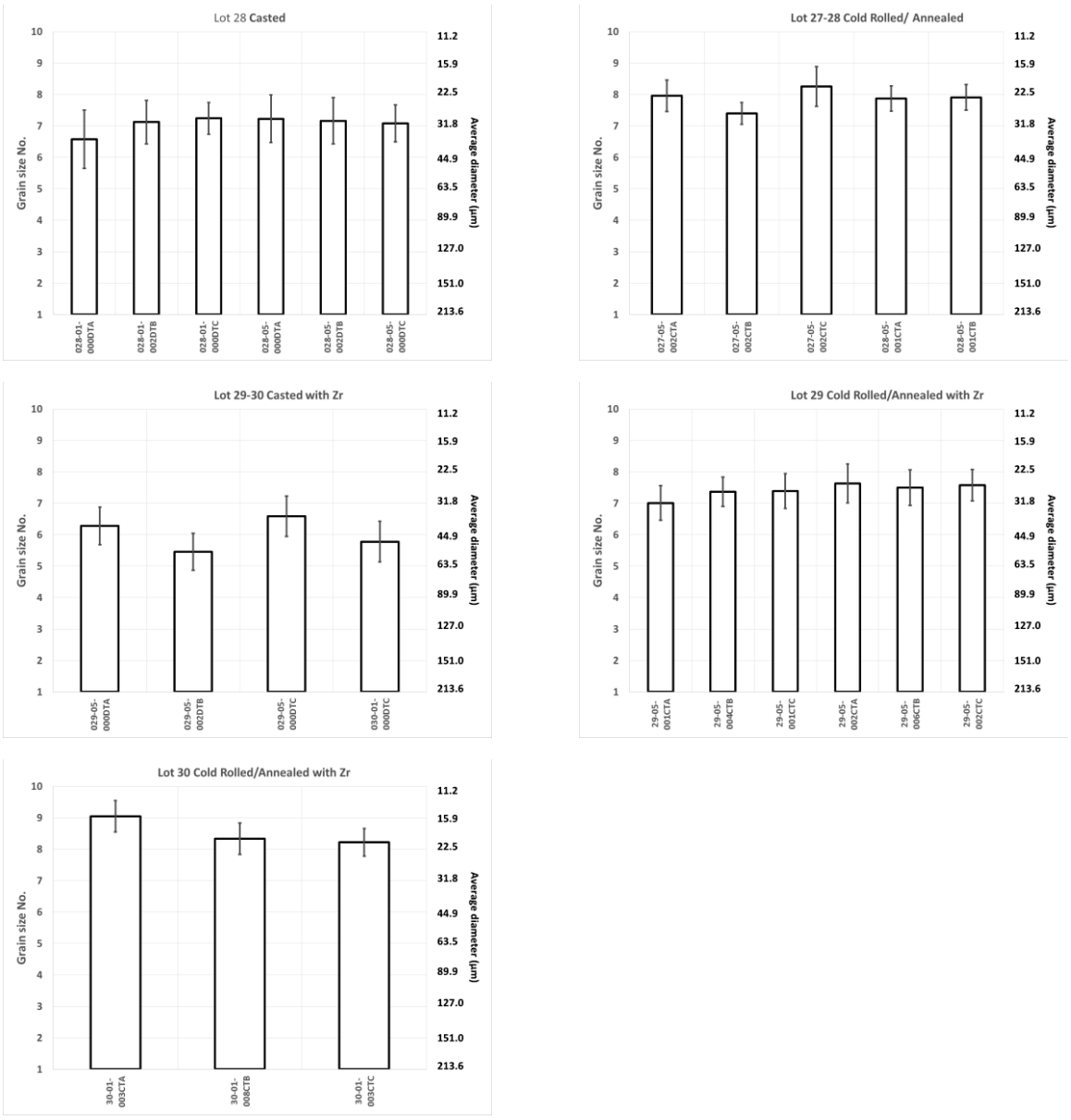

Figure 6. Summary of the grain size obtained from the analyses, each result is the average of the six analyzed sections.

3.2 Scanning Electron Microscopy

3.2.1 Mo distribution and chemical banding

Mo distribution was evaluated based on the EDX line scans monitoring U, and Mo composition. This was performed because the distribution was difficult to observe by imaging with the LABE detector. EDX analyses were performed to visualize the chemical banding, representing enriched region of Mo or U throughout the sample. This evaluation is important as low concentrations of Mo may lead to gamma-phase decomposition and also to ensure homogenous fissile material (i.e., U) distribution.

Elemental composition was collected for lines of 70–110 µm, with a step size of 1 µm. It has been deemed necessary to obtain the analyses of a higher number of points during this work. The work procedure has been updated to include at least 100 points [10]. This has been obtained by rotating the sample of 90 degrees, thus creating a larger area available for analysis. The images are collected at a 2048 × 1480 resolution, at 1000×, with the area available in both directions of 120 × 85 µm. The rotation is necessary to obtain the prescribed 100 µm. This new procedure has been applied starting from sample Number 79. This corresponds with the samples presenting the Zr coating and for which a higher number of analyses were requested. To limit the time for the analysis of each sample, the counting time was reduced from 60 to 20 s for each point, reaching counts over 30,000 for each point analyzed (vs 80,000 with 60 s). For the future samples a new procedure has been implemented which will use 100 points taken on the full length of the cross section, with a 60 s counting time followed by a large EDX analysis.

The Mo %wt. has been evaluated based on the described EDX analysis and corrected for the Au overlap from the coating. Presence of chemical banding was evaluated based on the trend observed in the elemental line scans. Examples of Mo line scan are shown in Figure 7. Sample 027-005-002CTA-Met1-FLongi shows a significant trend variation for the Mo concentration. The influence of carbides on elemental line scans can be observed for the example from sample 028-05-000DTA–Met3-BTrans in Figure 7. This is observed with a sudden drop in Mo weight concentration. Such values were discarded in our evaluation of the average Mo content. In Table 5, the Mo average value obtained from the multiple (70–120) points acquired on the line scan is reported, together with the range of variation. In the Table 5, it can be observed that the Mo composition variation is generally small (±0.25 %wt.). This may explain why chemical banding could not be observed by imaging in LABE mode. These values agree with expected and required Mo concentrations. Finally, in Table 5 the minimum and maximum value for Mo weight concentration are reported.

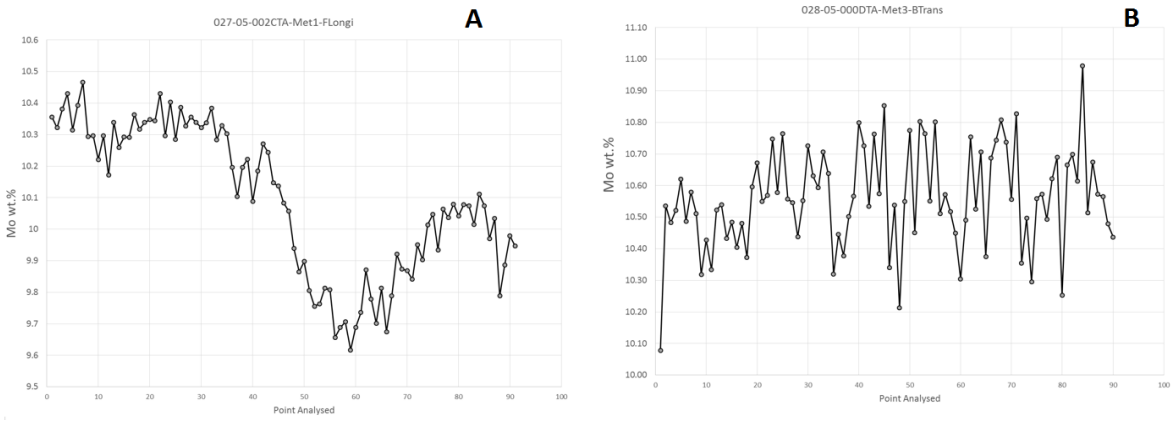

Figure 7. Example of Mo distribution for two samples (027-05-002CTA-MET1-FLongi A, and 028-05-000DTA-MET3-BTrans B). Image A shows evidence of chemical banding as a trend in the variation of the Mo content (%wt.). The second image B shows high variation, but no trend. The sudden drop in Mo content in the first point may be related to the presence of a small carbide in the proximity of the measurement spot.

Table 5. Mo elemental distribution obtained from EDX measurements. Chemical banding when detected is marked as Y, while N indicates no banding observed. Finally "?" indicates uncertainty in the evaluation of the presence of the banding.

No.	Sample Name	Mo average (%wt.)	Error (Std σ)	Mo variation	No points	Banding	No.	Sample Name	Mo average (%wt.)	Error (Std σ)	Mo Variation	Banding	No. points
1	028-01-000DTA	10.00	0.09	9.68–10.34	91	?	73	029-05-002DTB	9.88	0.16	9.55-10.20	Y	100
2		10.08	0.18	9.73–10.2	90	Y	74		10.00	0.18	9.66-10.34	Y	100
3		9.96	0.12	9.10–10.11	90	?	75		10.98	0.21	10.59-11.51	?	84
4		9.85	0.17	9.15–10.21	91	N	76		10.58	0.16	10.28-10.97	Y	120
5		10.04	0.23	9.55–9.99	91	Y	77		9.79	0.13	9.48-10.04	Y	100
6		9.78	0.10	9.31–10.41	77	?	78		10.07	0.11	9.50-10.31	?	100
7	028-01-002DTB	9.89	0.08	9.76–10.22	89	N	79	029-05-000DTC	9.75	0.09	9.49-9.98	N	105
8		9.93	0.08	9.59–10.06	89	N	80		9.64	0.07	9.39-9.92	N	100
9		9.82	0.08	9.55–9.95	91	N	81		9.79	0.08	9.54-9.98	N	108
10		9.78	0.08	9.43–10.00	91	N	82		9.76	0.08	9.60-10.03	N	107
11		9.83	0.08	10.13–10.98	82	N	83		9.73	0.07	9.52-9.97	N	115
12		10.56	0.17	9.65–10.05	91	N	84		9.74	0.08	9.46-9.99	N	107
13	028-01-000DTC	10.04	0.17	9.51–10.26	91	?	85	030-01-000DTC	9.76	0.09	9.56-10.04	Y	100
14		9.90	0.16	9.52–10.54	91	Y	86		9.85	0.09	9.67-10.10	N	100
15		9.92	0.12	9.62–10.11	91	N	87		9.92	0.11	9.57-10.31	N	107
16		9.89	0.10	9.62–10.17	90	Y	88		9.92	0.08	9.75-10.11	Y	105
17		10.00	0.10	9.72–10.13	91	Y	89		9.87	0.09	9.66-10.14	N	102
18		9.93	0.11	9.78–10.25	90	?	90		9.91	0.11	9.44-10.16	N	104
19	028-05-000DTA	10.61	0.32	9.78–10.82	89	N	91	029-05-0001CTA					
20		10.23	0.23	9.85–11.49	81	?	82						
21		10.90	0.14	9.87–10.80	76	?	83						
22		10.31	0.21	10.55–11.17	87	N	84						
23		10.69	0.14	10.10–11.04	89	N	95						
24		10.55	0.23	10.11–10.96	90	N	96						
25	028-05-002DTB	10.57	0.14	10.00–10.91	89	N	97	029-05-004CTB					
26		10.49	0.17	10.19–10.82	90	N	98						

No.	Sample Name	Mo average (%wt.)	Error (Std σ)	Mo variation	No points	Banding	No.	Sample Name	Mo average (%wt.)	Error (Std σ)	Mo Variation	Banding	No. points
27		9.78	0.07	9.59–10.04	90	Y	99						
28		9.78	0.10	9.61–10.00	90	N	100						
29		10.56	0.16	10.03–10.69	89	N	101						
30		10.35	0.14	10.08–10.98	88	N	102						
31	028-05-000DTC	9.61	0.11	9.63–10.13	90	Y	103	029-05-001CTC					
32		9.90	0.12	9.38–9.88	90	Y	104						
33		10.00	0.10	9.91–10.38	91	?	105						
34		10.13	0.11	9.51–10.19	90	?	106						
35		9.70	0.10	9.39–9.78	91	Y	107						
36		9.59	0.05	9.45–9.93	91	?	108						
37	027-05-002CTA	10.09	0.23	9.62–10.47	91	Y	109	029-05-002CTA					
38		10.05	0.11	9.51–10.28	89	?	110						
39		10.02	0.21	9.54–10.43	90	?	111						
40		10.01	0.14	9.34–10.24	91	Y	112						
41		9.97	0.11	9.70–10.20	85	N	113						
42		10.04	0.11	9.76–10.30	85	?	114						
43	027-05-002CTB	9.95	0.12	9.72–10.20	85	Y	115	029-05-006CTB					
44		9.65	0.11	9.42–9.89	85	Y	116						
45		9.61	0.15	9.38–9.90	85	Y	117						
46		9.81	0.20	9.53–10.25	85	Y	118						
47		9.55	0.09	9.32–9.77	85	Y	119						
48		9.74	0.16	9.4–10.1	85	Y	120						
49	027-05-002CTC	10.06	0.16	9.68–10.35	89	Y	121	029-05-002CTC					
50		10.03	0.16	9.44–10.42	90	?	122						
51		9.86	0.12	9.64–10.13	82	Y	123						
52		10.03	0.35	9.61–11.33	82	?	124						
53		10.00	0.15	9.66–10.37	83	Y	125						
54		9.96	0.22	9.63–10.45	83	Y	126						

No.	Sample Name	Mo average (%wt.)	Error (Std σ)	Mo variation	No points	Banding	No.	Sample Name	Mo average (%wt.)	Error (Std σ)	Mo Variation	Banding	No. points
55	028-05-001CTA	10.38	0.47	9.58–11.14	85	Y	127	030-01-003CTA					
56		10.64	0.14	10.27–10.92	84	N	128						
57		10.51	0.18	10.10–10.97	85	?	129						
58		10.58	0.14	10.16–10.98	85	N	130						
59		10.73	0.14	10.34–11.18	85	?	131						
60		9.93	0.19	9.57–10.34	85	Y	132						
61	028-05-001CTB	9.76	0.21	9.36–10.21	89	?	133	030-01-008CTB					
62		9.84	0.11	9.60–10.06	85	?	134						
63		10.32	0.35	9.66–10.972	84	Y	135						
64		9.93	0.14	9.61–10.21	85	Y	136						
65		9.81	0.19	9.30–10.15	85	Y	137						
66		9.68	0.15	9.34–9.93	85	Y	138						
67	029-05-000DTA	9.94	0.12	9.56–10.39	100	?	139	030-01-003CTC					
68		9.64	0.09	9.39–9.83	100	?	140						
69		9.51	0.35	8.93–10.07	100	Y	141						
70		10.72	0.16	10.36–11.10	100	Y	142						
71		9.97	0.16	9.38–10.48	105	?	143						
72		9.88	0.25	9.36–10.38	119	Y	144						

3.2.2 Carbide evaluation

As explained, carbide evaluation is important because it can influence the mechanical behavior of the fuel (i.e., its brittle nature); moreover, near extensive carbide regions, gamma-phase decomposition is observed. Therefore, evaluating carbide distribution and volume fraction is essential to evaluate further performance in the reactor. Carbides can easily be identified based on their darker contrast with respect to the matrix when using the LABE detector, as shown in Figure 8. Carbide volume-fraction (Vi) evaluation was performed based on the SEM images, obtained with the LABE detector at 250×, following the ASTM E562-11 procedure [8] and using a rectangular grid of ~700 points. This grid was created using ImageJ software [10] and superimposed on the images visualized through the computer screen. Manual counting was performed as described in Reference [8]. In this method, the operator is required to count the number of carbides that fall on the grid (Pt). Grid points falling on the carbides are counted as one, while points falling on the carbide boundary were counted as one half, as prescribed by Reference [8]. This number is divided by the total number of grid points yielding (Pt) a point fraction, as shown in the following equation (Equation 1). The average (Equation 2) point fraction for the images analyzed gives an estimation of the carbide volume fraction.

$$P_p(i) = \frac{P_i}{P_t} \tag{1}$$

$$\overline{P_p} = \frac{1}{n}\sum_{i=1}^{n} P_p\ (i) \tag{2}$$

For comparison, ImageJ software was used also for carbide fraction determination by image analyses. This was performed following the ASTM E1245-03 Reference [9]. Carbides are again identified based on their gray scale with respect to the fuel matrix and based on thresholding of the image and conversion to a binary (black/white) image, as shown in Figure 9. The procedure for the ImageJ method included the following steps, utilized with a macro automation sequence, and summarized in Figure 10: the SEM images for analyses were opened and cropped to eliminate the label and other possible artifacts (polishing compounds, shadowing etc.), which could not be eliminated solely by the threshold method. A threshold for the figure was then established using two methods: operator-controlled threshold and automatic threshold. The values obtained from each applied threshold are comparable within the standard deviation. However, a slightly higher relative accuracy was obtained using the operator-controlled threshold method. The images were then processed using the binary module using the "fill holes" feature. The "analyze particles" module was applied using the include-holes feature. Carbides with a dimension less than 5 pixels were considered noise and excluded based on operator observation of SEM images and a minimum-size precipitate observable. Following the particle-count analyses, a list of particle size and position were exported, together with the output figure, showing carbide edges outlined. All images were checked individually by an operator to identify any miscount, and if necessary, threshold and cropping were refined to exclude or include points of interest. A summary of the results is shown in Figure 11 and Table 6 for volume-fraction evaluation. All samples had a low carbide content under 1.5%. However, a large standard deviation was observed for both methods; this may indicate inhomogeneous carbide distribution.

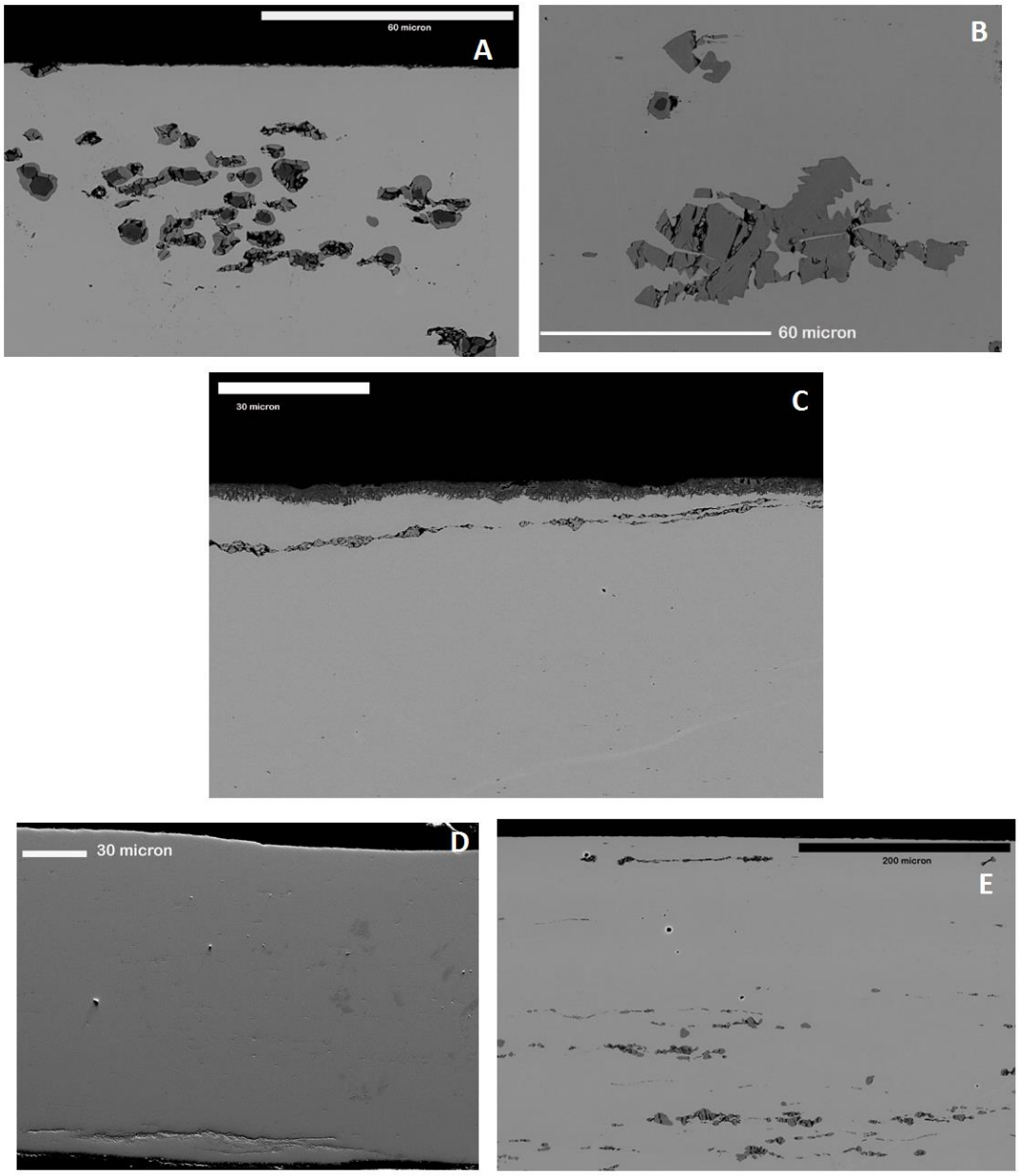

Figure 8. Examples of carbides dimension and distribution. In image A and B, large carbides over 10 µm can be seen (027-05-002CTB-Met2-MTrans A, 028-01-000DTA-Met2-MTrans B). Sample 028-05-001CTA-Met3-BLongi, in image C, shows a long carbide and oxide skin. In images C and D carbide strings over 400 µm long are observed (028-01-000DTA-Met2-MTrans D, and 027-05-002CTB-Met2-MLongi E).

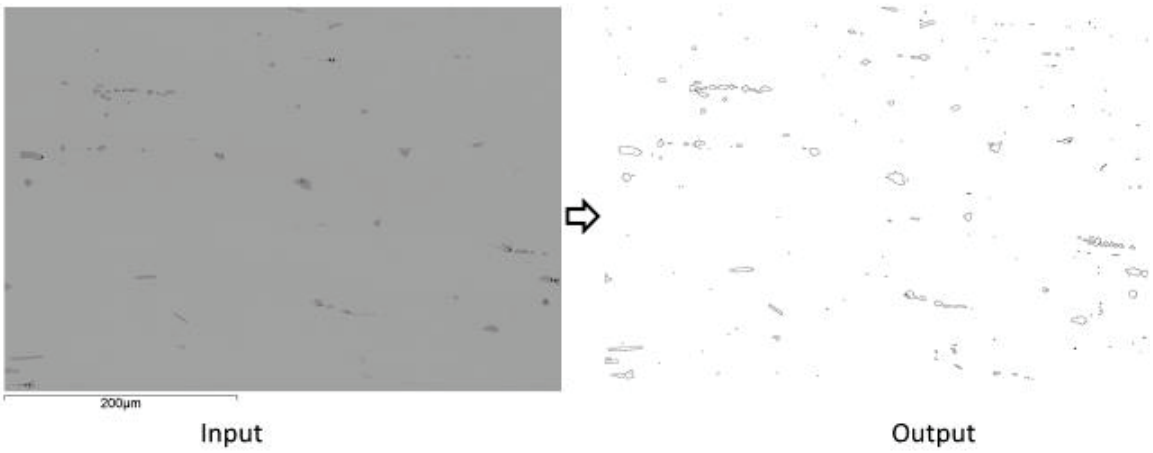

Figure 9. Example of the input and output for the carbide evaluation performed by Image analyses.

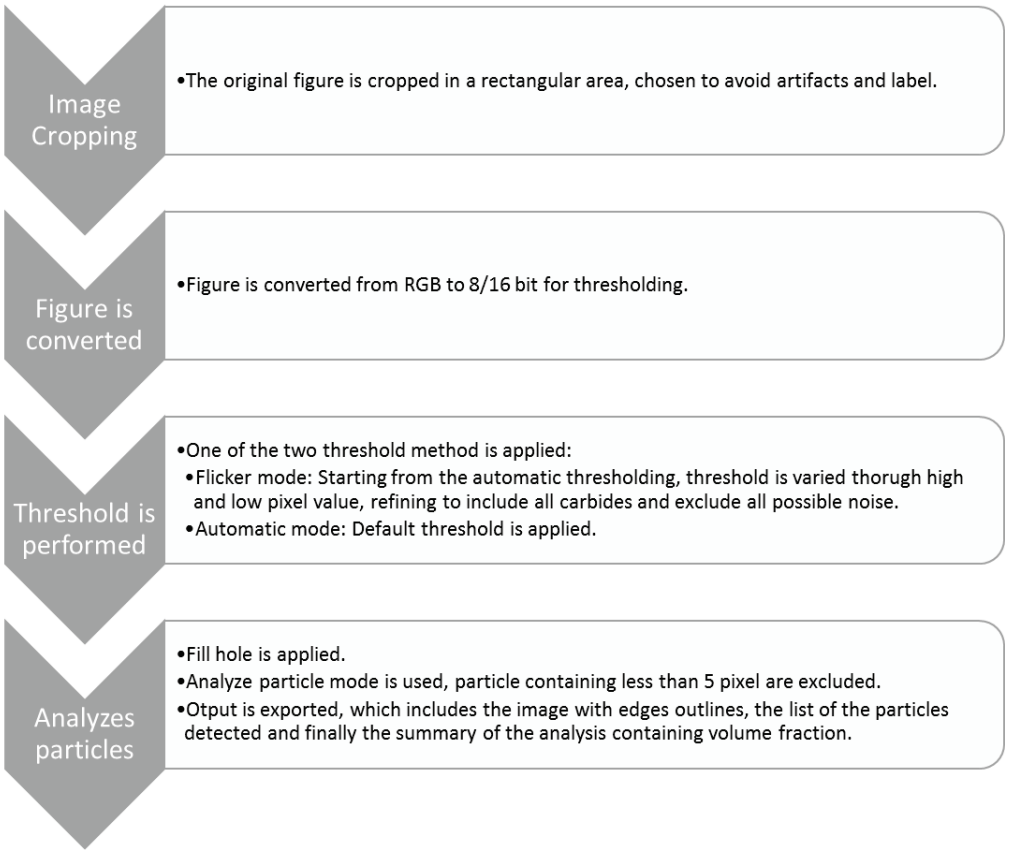

Figure 10. Scheme summarizing the steps performed in image analyses with the ImageJ analysis software.

Table 6. Carbide volume fraction (Vi) results. Blank space in the table indicates that the analyses need still to be performed.

No.	Sample Name	Vf (%) IA	Error (Std σ)	95% CI	Vf (%) Grid	Error (Std σ)	95% CI	No.	Sample Name	Vf (%) IA	Error (Std σ)	95% CI	Vf (%) Grid	Error (Std σ)	95% CI
1		0.45	0.12	0.08	0.61	0.27	0.20	73		1.00	0.44	0.41	0.96	0.56	0.43
2		0.48	0.13	0.10	0.47	0.22	0.17	74		0.82	0.19	0.16	0.90	0.30	0.27
3	028-01-000DTA	0.86	0.45	0.32	0.81	0.45	0.32	75	029-05-002DTB	0.91	0.32	0.25	0.76	0.31	0.24
4		1.01	1.01	0.72	0.93	1.11	0.79	76		0.64	0.19	0.18	0.65	0.15	0.13
5		0.57	0.14	0.11	0.46	0.10	0.08	77		0.90	0.21	0.19	0.96	0.35	0.29
6		0.66	0.13	0.09	0.64	0.18	0.13	78		0.89	0.17	0.13	0.89	0.17	0.13
7		0.58	0.24	0.20	0.72	0.33	0.26	79		0.72	0.11	0.08	0.71	0.20	0.16
8		0.69	0.16	0.20	0.67	0.24	0.20	80		0.65	0.07	0.06	0.60	0.26	0.22
9	028-01-002DTB	0.55	0.13	0.10	0.77	0.23	0.16	81	029-05-000DTC	0.70	0.13	0.10	0.61	0.18	0.13
10		0.49	0.09	0.06	0.57	0.22	0.15	82		0.72	0.09	0.07	0.50	0.13	0.10
11		0.46	0.14	0.12	0.70	0.27	0.21	83		0.74	0.14	0.13	0.54	0.14	0.12
12		0.56	0.13	0.11	0.79	0.30	0.25	84		0.62	0.12	0.10	0.62	0.28	0.23
13		0.49	0.13	0.11	0.78	0.19	0.15	85		0.68	0.13	0.13	0.70	0.36	0.30
14		0.52	0.17	0.15	0.59	0.20	0.15	86		0.68	0.21	0.16	0.62	0.17	0.14
15	028-01-000DTC	0.48	0.22	0.19	0.54	0.32	0.25	87	030-01-000DTC	0.70	0.17	0.13	0.60	0.31	0.24
16		0.54	0.19	0.16	0.70	0.16	0.12	88		0.76	0.16	0.12	0.84	0.44	0.31
17		0.52	0.25	0.21	0.61	0.20	0.15	89		0.69	0.13	0.12	0.54	0.29	0.25
18		0.57	0.22	0.18	0.57	0.38	0.29	90		0.71	0.13	0.10	0.70	0.17	0.12
19		1.36	0.50	0.42	0.74	0.35	0.33	91							
20		1.21	0.34	0.43	1.12	0.23	0.28	82							
21	028-05-000DTA	0.58	0.16	0.17	0.59	0.16	0.17	83	029-05-0001CTA						
22		0.57	0.33	0.41	0.67	0.23	0.20	84							
23		1.04	0.51	0.47	0.88	0.59	0.54	95							
24		0.65	0.38	0.33	0.67	0.32	0.23	96							
25		0.81	0.17	0.18	0.70	0.25	0.26	97							
26		0.82	0.28	0.29	0.83	0.30	0.37	98							
27	028-05-002DTB	0.71	0.15	0.11	0.78	0.26	0.20	99	029-05-004CTB						
28		0.65	0.28	0.24	0.90	0.23	0.18	100							
29		0.80	0.13	0.16	0.69	0.18	0.19	101							
30		0.63	0.13	0.16	0.71	0.39	0.49	102							
31		1.05	0.28	0.23	0.61	0.27	0.20	103							
32		0.90	0.22	0.18	0.78	0.28	0.22	104							
33	028-05-000DTC	0.76	0.29	0.20	0.61	0.27	0.20	105	029-05-001CTC						
34		0.87	0.31	0.26	0.90	0.17	0.13	106							
35		0.59	0.18	0.13	0.70	0.31	0.23	107							
36		0.99	0.45	0.48	0.83	0.37	0.34	108							
37		1.46	0.34	1.14	1.28	0.37	0.26	109							
38		1.47	0.29	1.23	1.02	0.31	0.29	110							
39	027-05-002CTA	1.77	0.50	1.50	1.71	0.61	0.55	111	029-05-002CTA						
40		1.35	0.20	0.17	1.21	0.30	0.26	112							
41		1.31	0.36	1.07	1.56	0.49	0.35	113							
42		1.59	0.15	1.29	1.40	0.22	0.17	114							
43	027-05-002CTB	1.83	0.46	1.53	1.67	0.55	0.43	115	029-05-006CTB						
44		1.69	0.20	1.30	1.57	0.33	0.28	116							

No.	Sample Name	Vf (%) IA	Error (Std σ)	95% CI	Vf (%) Grid	Error (Std σ)	95% CI	No.	Sample Name	Vf (%) IA	Error (Std σ)	95% CI	Vf (%) Grid	Error (Std σ)	95% CI
45		1.36	0.43	1.25	1.15	0.54	0.41	117							
46		1.46	0.24	1.22	1.40	0.54	0.42	118							
47		1.60	0.61	1.34	1.37	0.39	0.27	119							
48		1.55	0.28	1.30	1.05	0.40	0.31	120							
49		1.80	0.60	1.67	1.52	0.71	0.66	121							
50		1.74	0.55	1.61	1.58	0.29	0.23	122							
51	027-05-002CTC	1.83	0.68	1.70	1.61	0.78	0.60	123	029-05-002CTC						
52		1.59	0.16	1.33	1.50	0.40	0.33	124							
53		1.72	0.54	1.32	1.58	0.66	0.51	125							
54		1.45	0.10	1.11	1.29	0.30	0.23	126							
55		1.02	0.54	0.73	1.02	0.53	0.38	127							
56		1.10	0.14	0.92	1.10	0.44	0.28	128							
57	028-05-001CTA	0.89	0.19	0.88	1.01	0.56	0.43	129	030-01-003CTA						
58		1.06	0.66	0.74	0.88	0.35	0.27	130							
59		0.69	0.18	0.58	0.83	0.20	0.16	131							
60		0.80	0.14	0.62	0.77	0.37	0.28	132							
61		0.80	0.19	0.61	0.81	0.39	0.30	133							
62		0.90	0.20	0.68	0.83	0.34	0.29	134							
63	028-05-001CTB	0.84	0.21	0.64	0.85	0.25	0.21	135	030-01-008CTB						
64		0.77	0.10	0.59	0.68	0.36	0.30	136							
65		0.78	0.22	0.60	0.54	0.12	0.09	137							
66		0.77	0.23	0.71	0.57	0.23	0.19	138							
67		0.66	0.24	0.18	0.79	0.39	0.30	139							
68		0.93	0.46	0.38	0.71	0.42	0.28	140							
69	029-05-000DTA	0.64	0.24	0.20	0.61	0.19	0.15	141	030-01-003CTC						
70		0.83	0.20	0.16	0.75	0.30	0.23	142							
71		0.85	0.28	0.20	0.81	0.41	0.29	143							
72		0.81	0.25	0.19	0.79	0.29	0.22	144							

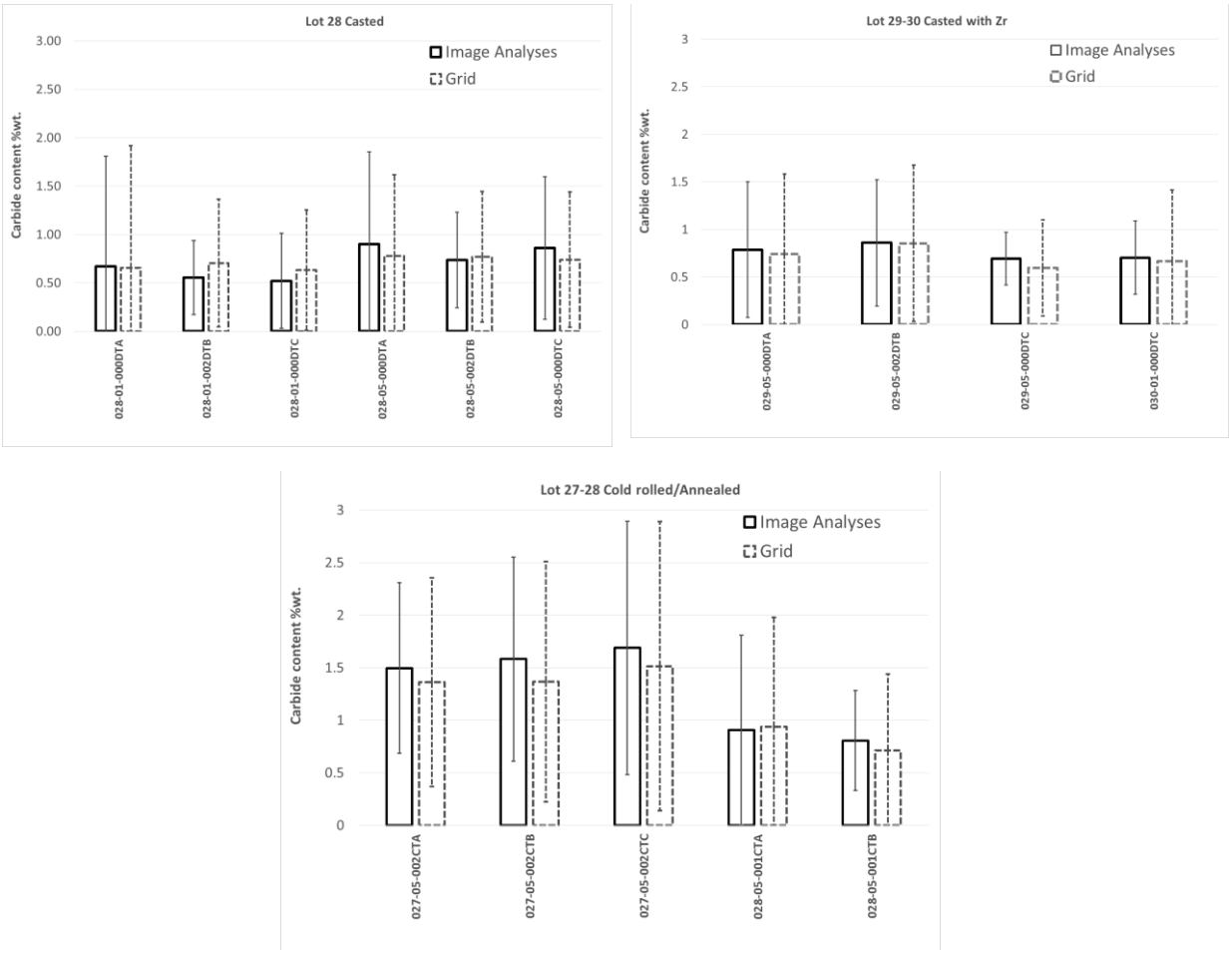

Figure 11. Graph summarizing the carbide volume fraction for each foil, averaged on the six sections analyzed.

The carbide dimensions were also analyzed. The carbide dimensions are reported in Table 7. The average area was between 3 and 12 μm^2. Submicron carbides may be present in the sample, but may not have been quantitatively counted as they are difficult to distinguish from polishing artifacts and noise. The minimum dimension observable through these analyses was 280 nm^2. In some samples, long strings of carbides, up to 2 mm in length, were observed as shown in Figure 8. Usually in the presence of such extensive carbide precipitates, cracks were also observed. The presence of long carbide chains explains the high variation on the carbide dimensions, reaching also 1500 μm^2.

Table 7. Summary of particle size distribution obtained from ImageJ evaluation.

No.	Sample Name	Average area (μm^2)	Error (Std σ)	Min/Max area (μm^2)	Median	No.	Sample Name	Average area (μm^2)	Error (Std σ)	Min/Max area (μm^2)	Median
1	028-01-000DTA	2.9	8.5	0.28/88	0.39	73	029-05-002DTB	12	41	0.28/993	2.0
2		3.3	12	0.28/186	0.39	74		8.6	22	0.28/212	1.0
3		4.5	52	0.28/2361	0.39	75		7.6	33	0.28/806	0.95
4		3.5	20	0.28/837	0.33	76		7.0	17	0.28/192	0.84
5		2.7	11	0.28/329	0.39	77		9.6	37	0.28/1085	0.95

No.	Sample Name	Average area (μm^2)	Error (Std σ)	Min/Max area (μm^2)	Median	No.	Sample Name	Average area (μm^2)	Error (Std σ)	Min/Max area (μm^2)	Median
6		3.1	9.7	0.28/174	0.39	78		8.7	19	0.28/234	0.89
7	028-01-002DTB	3.5	8.1	0.28/116	0.50	79	029-05-000DTC	7.7	12	0.28/170	2.4
8		3.7	9.1	0.28/121	0.44	80		8.3	12	0.28/112	2.7
9		3.7	8.2	0.28/69	0.44	81		5.7	9.6	0.28/110	1.2
10		4.3	9.8	0.28/82	0.44	82		6.1	13	0.28/265	1.1
11		6.2	9.4	0.28/100	1.5	83		5.7	10	0.28/97.8	1.0
12		4.3	9.8	0.28/81	0.5	84		5.7	10	0.28/80	1.1
13	028-01-000DTC	3.0	12	0.28/297	0.39	85	030-01-000DTC	5.7	11	028/167	1.1
14		2.8	9.5	0.28/155	0.39	86		7.0	14	0.28/270	0.84
15		3.1	11	0.28/174	0.39	87		9.5	15	0.28/166	2.2
16		2.5	8.6	0.28/103	0.39	88		12	19	0.28/194	3.6
17		3.1	10	0.28/210	0.39	89		6.1	13	0.28/220	0.67
18		3.1	13	0.28/317	0.39	90		6.7	12	0.28/107	0.89
19	028-05-000DTA	12[b]	63	0.71/140	1.7	91	029-05-0001CTA				
20		2.8[3]	9.6	0.71/313	1.1	82					
21		6.7[3]	25	0.71/402	1.4	83					
22		5.9[3]	36	0.71/965	1.1	84					
23		2.2	11	0.28/355	0.39	95					
24		2.7	17	0.28/591	0.39	96					
25	028-05-002DTB	7.0[3]	10	0.70/144	3.5	97	029-05-004CTB				
26		4.9[3]	8.3	0.70/93	1.5	98					
27		4.5	9.3	0.28/102	0.93	99					
28		2.9	7.5	0.28/121	0.56	100					
29		6.4[3]	8.1	0.70/53	3.5	101					
30		5.8[3]	10	0.70/150	2.1	102					
31	028-05-000DTC	5.3	15	0.28/421	0.56	103	029-05-001CTC				
32		6.0	20	0.28/526	0.62	104					
33		5.3	22	0.28/727	0.50	105					
34		6.6	33	0.28/1394	0.50	106					
35		8.2	50	0.28/1430	0.50	107					
36		4.6	13	0.28/164	0.45	108					
37	027-05-002CTA	10	22	0.28/232	2.4	109	029-05-002CTA				

b. Different resolution of image minimum detectable size 0.7 μm.

No.	Sample Name	Average area (μm^2)	Error (Std σ)	Min/Max area (μm^2)	Median	No.	Sample Name	Average area (μm^2)	Error (Std σ)	Min/Max area (μm^2)	Median
38		8.5	16	0.28/327	3.2	110					
39		6.6	17	0.28/351	1.5	111					
40		8.4	17	0.28/260	2.5	112					
41		6.2	15	0.28/261	1.6	113					
42		7.8	14	0.28/216	2.6	114					
43	027-05-002CTB	9.2	23	0.28/470	2.6	115	029-05-006CTB				
44		7.5	17	0.28/463	2.4	116					
45		7.0	17	0.28/342	1.5	117					
46		7.3	14	0.28/150	2.2	118					
47		9.7	17	0.28/168	3.2	119					
48		8.6	14	0.28/154	2.6	120					
49	027-05-002CTC	9.7	31	0.28/774	2.4	121	029-05-002CTC				
50		8.2	29	0.28/1313	2.5	122					
51		3.6	10	0.28/179	1.2	123					
52		8.0	19	0.28/440	2.0	124					
53		11	25	0.28/293	2.8	125					
54		8.4	15	0.28/146	2.9	126					
55	028-05-001CTA	4.4	21	0.28/936	0.67	127	030-01-003CTA				
56		4.6	11	0.28/176	0.78	128					
57		4.7	27	0.28/749	0.56	129					
58		4.2	9.4	0.28/121	0.62	130					
59		3.3	9.4	0.28/160	0.56	131					
60		4.6	14	0.28/436	0.67	132					

No.	Sample Name	Average area (μm²)	Error (Std σ)	Min/Max area (μm²)	Media n	No.	Sample Name	Average area (μm²)	Error (Std σ)	Min/Max area (μm²)	Media n
61	028-05-001CTB	4.0	10	0.28/156	0.67	133	030-01-008CTB				
62		4.6	14	0.28/467	0.67	134					
63		4.4	16	0.28/497	0.56	135					
64		3.3	8.8	0.28/115	0.56	136					
65		3.4	9.9	0.28/177	0.62	137					
66		3.6	11	0.28/376	0.56	138					
67	029-05-000DTA	6.9	16	0.28/194	0.81	139	030-01-003CTC				
68		7.5	21	0.28/336	0.73	140					
69		6.7	18	0.28/246	0.73	141					
70		8.5	22	0.28/191	0.67	142					
71		8.3	48	0.28/1752	0.67	143					
72		7.6	20	0.28/263	0.67	144					

Finally, EDX mapping was used to evaluate the composition of the carbides, revealing different oxygen content in the precipitates, as shown in Figure 12. For EDX mapping, similar analytical conditions were used, and generally, 100–150 frames were acquired. Although quantitative analyses are generally unreliable for light elements such as C and O, due to intrinsic nature of EDX measurement, point analyses were performed to qualitatively indicate the different character of the oxy-carbides present in these samples (Figure 13). The point analyses show that the precipitates may contain only U-C or a U-C-O mixture. These could be differentiated also simply by the different contrast observed in the LABE mode because the U-C-O presents a darker color with respect to the U-C precipitates.

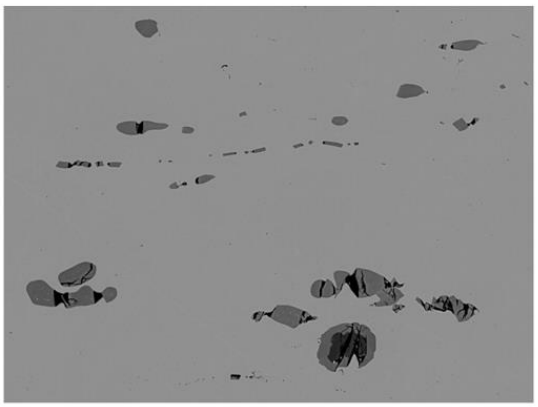

Electron Image 1

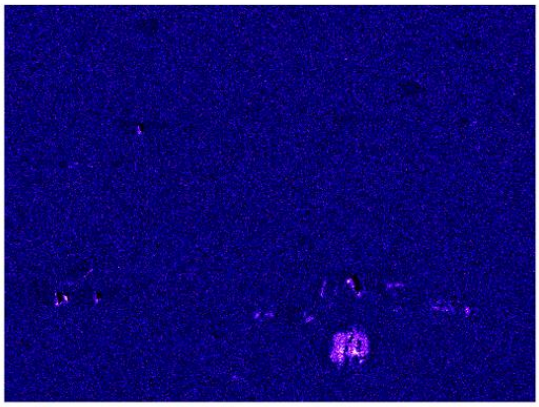

O Ka1

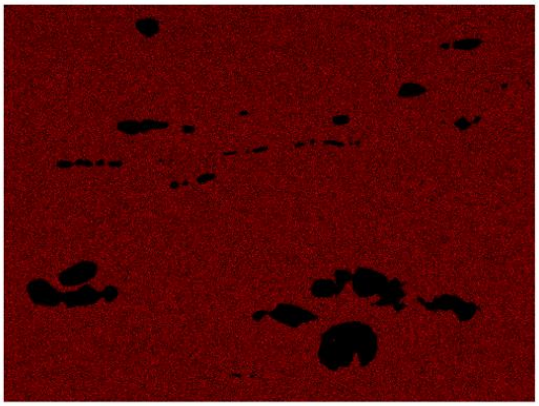

Mo La1

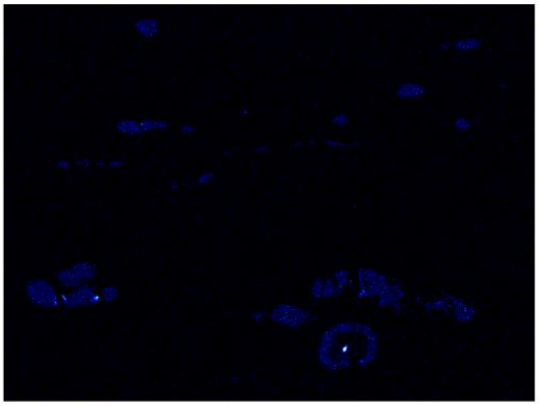

C Ka1_2

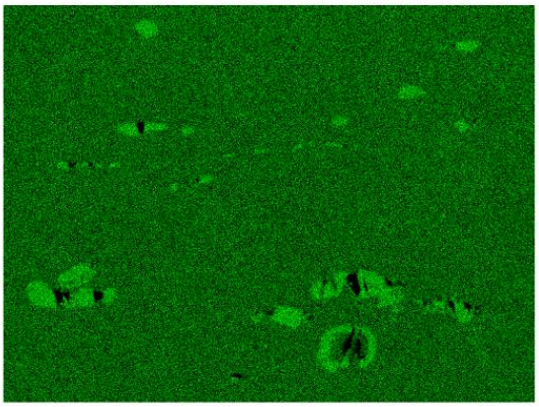

U Ma1

Figure 12. An example of EDX mapping (027-05-002CTA -MET2-MLongi) performed on the carbide precipitates and showing the presence of U-C-O and/or U-C. The darker region in the carbides shows the presence of higher concentration of oxygen. Mo chemical banding cannot be observed even with long EDX mapping times.

Spectrum	C	O	Mo	U
Spectrum 1	10.99	7.01	5.69	76.31
Spectrum 2	11.13	8.35	3.83	76.69
Spectrum 3	7.53	10.70		81.77
Spectrum 4	7.34	10.65		82.01
Spectrum 5	7.40	10.76		81.84
Spectrum 6	9.14	0.22		90.64
Spectrum 7	9.12			90.82
Spectrum 8	9.20			90.80
Spectrum 9	10.44	2.74	6.02	80.80
All Results in weight %				

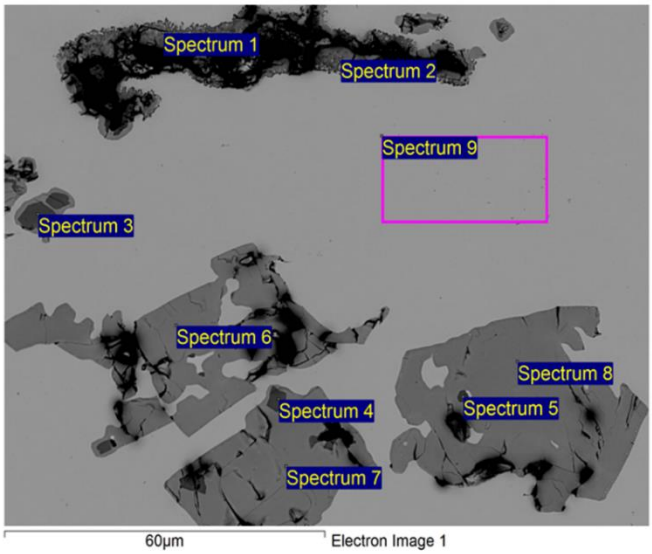

Figure 13. Example of an elemental analyses on a sample (028-01-000DTA-MET3-BLongi) showing different U-C-O composition. In Spectra 1 and 2, the presence of Mo could be related to the crack showing material under or at the indented character of that carbide, thus measuring part of the matrix nearby.

3.2.3 Gamma phase decomposition

Some indication of phase decomposition may have been observed by SEM in some samples (Figure 14 and Figure 15), as summarized in Table 8. However, its limited amount and localized extension may be why observation of gamma-phase decomposition by optical microscopy is not possible. Gamma phase decomposition was observed by SEM as the well-known lamellar structure and was observed especially near the oxy-carbide precipitates and/or skin, (Figure 14) and near the Zr interaction layer (Figure 15). These lamellar structures were analyzed WDX line scans (Figure 16) showed Mo depletion, which could confirm that they indeed represent gamma-phase decomposition. This feature, as previously explained, is important because gamma-phase decomposition can lead to the formation of alpha phase, which can in turn lead to anisotropic swelling during reactor irradiation, influencing reactor performance and possibly leading to failure.

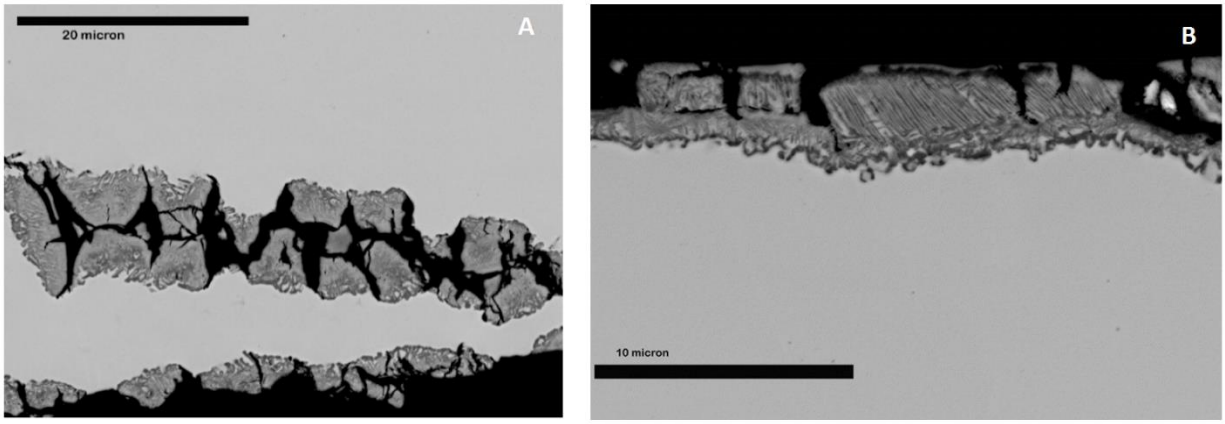

Figure 14. An example of incipit gamma phase decomposition in the samples at the border of the precipitates (A 028-01-002DTB-MET1-FTrans) and at the oxide skin (B027-05-002CTB-MET1-FTrans).

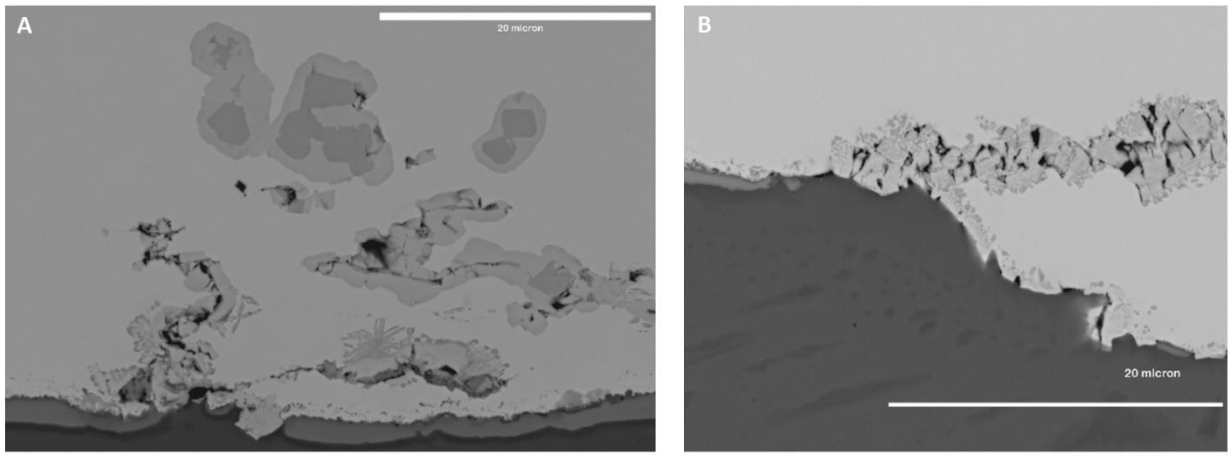

Figure 15. An example of incipit gamma phase decomposition within the samples in the presence of the Zr interaction layer (A 030-01-000DTC -Met3-BLongi) and carbides (B 029-05-000DTA-Met1-FLongi).

Table 8. Summary of samples in which gamma-phase decomposition was observed. Y indicates that such structure was observed while N/A indicates samples in which the lamellar feature was not detected. S indicates that a small region could be identified having gamma-phase decomposition.

No.	Sample Name	γ phase dec.	No.	Sample Name	γ phase dec.	No.	Sample Name	γ phase dec.	No.	Sample Name	γ phase dec.
1		Y	37		Y	73		Y	109		
2		Y	38		Y	74		Y	110		
3	028-01-	Y	39	027-05-	Y	75	029-05-	Y	111	029-05-	
4	000DTA	Y	40	002CTA	Y	76	002DTB	Y	112	002CTA	
5		Y	41		Y	77		Y	113		
6		Y	42		Y	78		Y	114		
7		Y	43		Y	79		Y	115		
8	028-01-	Y	44	027-05-	Y	80	029-05-	Y	116	029-05-	
9	002DTB	Y	45	002CTB	N/A	81	000DTC	Y	117	006CTB	
10		Y	46		Y	82		Y	118		

No.	Sample Name	γ phase dec.	No.	Sample Name	γ phase dec.	No.	Sample Name	γ phase dec.	No.	Sample Name	γ phase dec.
11		Y	47		Y	83		Y	119		
12		Y	48		Y	84		Y	120		
13		Y	49		Y	85		Y	121		
14		Y	50		Y	86		Y	122		
15	028-01-000DTC	Y	51	027-05-002CTC	Y	87	030-01-000DTC	Y	123	029-05-002CTC	
16		N/A	52		Y	88		Y	124		
17		Y	53		Y	89		Y	125		
18		Y	54		Y	90		Y	126		
19		Y	55		Y	91			127		
20		Y	56		Y	82			128		
21	028-05-000DTA	N/A	57	028-05-001CTA	Y	83	029-05-0001CTA		129	030-01-003CTA	
22		N/A	58		Y	84			130		
23		Y	59		Y	95			131		
24		Y	60		Y	96			132		
25		N/A	61		S	97			133		
26		Y	62		Y	98			134		
27	028-05-002DTB	Y	63	028-05-001CTB	S	99	029-05-004CTB		135	030-01-008CTB	
28		Y	64		N/A	100			136		
29		Y	65		Y	101			137		
30		Y	66		Y	102			138		
31		Y	67		Y	103			139		
32		N/A	68		Y	104			140		
33	028-05-000DTC	Y	69	029-05-000DTA	Y	105	029-05-1CTC		141	030-01-003CTC	
34		Y	70		Y	106			142		
35		Y	71		Y	107			143		
36		Y	72		Y	108			144		

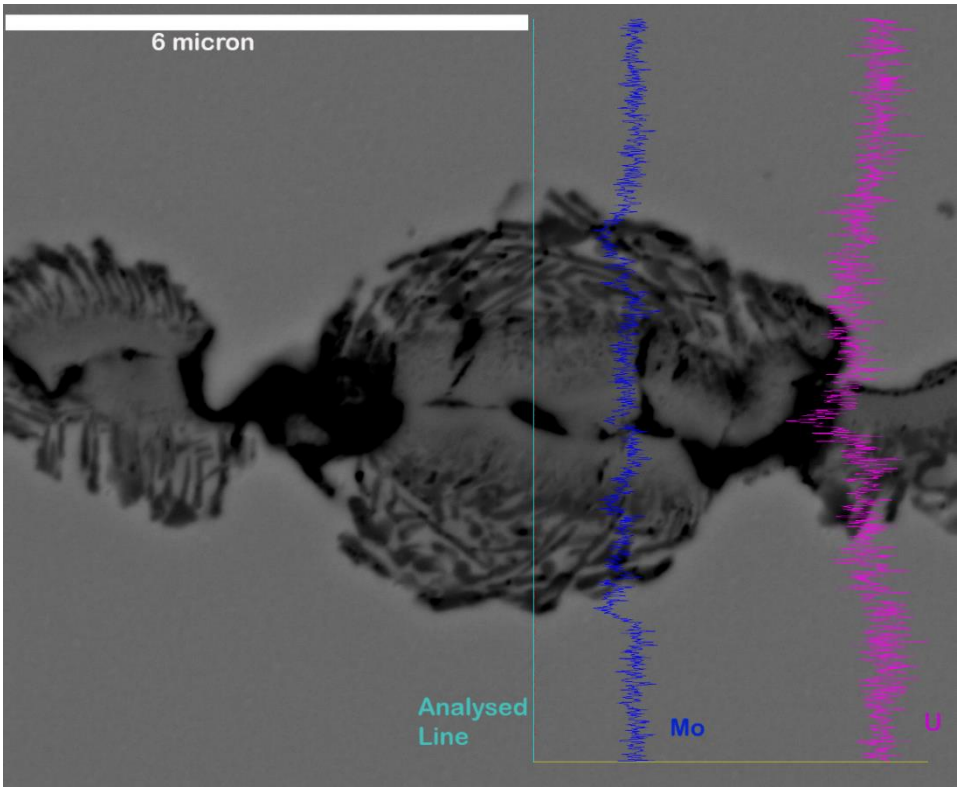

Figure 16. EDX line scan showing that Mo is depleted (blue line) in the lamellar microstructure, potentially indicating the gamma phase decomposition near the carbides.

3.2.4 Thickness determination

Information documenting the dimensional specification of the fabricated foils is important to qualify the precision of the fabrication process. Thickness was analyzed based on SEM images collected in low-magnification mode (45–50×) with the LEI detector. The thickness of the foil was measured in at least 10 locations, as required in Reference [4]. Measurements were taken along the full length of the sample and at 100 µm apart. A summary of the thickness measured is reported in Table 9.

Table 9. Summary of thickness determination for the foil.

No	Sample Name	Length (µm)	Error (Std σ)	No	Sample Name	Length (µm)	Error (Std σ)	No	Sample Name	Length (µm)	Error (Std σ)	No	Sample	Length (µm)	Error (Std σ)
1		1344	38	37		690	12	73		1507	28	109			
2		1407	31	38		689	12	74		1447	46	110			
3	028-01-000DTA	1481	32	39	027-05-002CTA	722	16	75	029-05-002DTB	1495	40	111	029-05-002CTA		
4		1487	36	40		724	6	76		1543	25	112			
5		1409	23	41		623	13	77		1476	17	113			
6		1326	47	42		633	5	78		1518	16	114			
7		1471	34	43		684	4	79		1446	36	115			
8		1485	36	44		681	7	80		1434	51	116			
9	028-01-002DTB	1431	42	45	027-05-002CTB	709	3	81	029-05-000DTC	1609	42	117	029-05-006CTB		
10		1439	43	46		710	4	82		1606	41	118			
11		1535	48	47		698	5	83		1572	47	119			
12		1562	31	48		705	5	84		1589	16	120			
13	028-01-000DTC	1441	55	49	027-05-002CTC	718	6	85	030-01-000DTC	1448	25	121	029-05-002CTC		
14		1433	17	50		729	6	86		1497	28	122			

No	Sample Name	Length (µm)	Error (Std σ)	No	Sample Name	Length (µm)	Error (Std σ)	No	Sample Name	Length (µm)	Error (Std σ)	No	Sample	Length (µm)	Error (Std σ)
15		1468	43	51		755	5	87		1554	21	123			
16		1476	29	52		754	5	88		1530	12	124			
17		1475	28	53		724	11	89		1607	24	125			
18		1491	34	54		737	6	90		1569	20	126			
19		1614	27	55		713	10	91				127			
20		1607	30	56		691	5	82				128			
21	028-05-	1635	50	57	028-05-	726	6	83	029-05-			129	030-01-		
22	000DTA	1658	42	58	001CTA	722	6	84	0001CTA			130	003CTA		
23		1423	25	59		713	7	95				131			
24		1548	25	60		715	5	96				132			
25		1537	14	61		710	4	97				133			
26		1482	11	62		698	7	98				134			
27	028-05-	1512	22	63	028-05-	725	6	99	029-05-			135	030-01-		
28	002DTB	1514	16	64	001CTB	728	5	100	004CTB			136	008CTB		
29		1438	20	65		725	5	101				137			
30		1451	27	66		729	3	102				138			
31		1481	23	67		1449	44	103				139			
32		1462	24	68		1446	45	104				140			
33	028-05-	1443	43	69	029-05-	1480	41	105	029-05-			141	030-01-		
34	000DTC	1433	25	70	000DTA	1438	15	106	1CTC			142	003CTC		
35		1495	30	71		1413	26	107				143			
36		1486	38	72		1375	29	108				144			

3.2.5 Zr layer evaluation

The Zr layer was also evaluated for composition and thickness. This layer is important as it acts as a diffusion barrier and prevents formation of an interaction layer between the fuel and the Al cladding, which can to lead to cladding failure during irradiation [11]. Zr thickness was evaluated following the revised test plan [12], which requires the determination of the average of Zr layer thickness from 10 different locations at least 100 µm apart (using at least two 200×, backscatter-electron images). For our evaluation, images were taken with a 250× magnification, acquired with the LABE detector. The starting point for this measurement was chosen by excluding the UZr_2 interaction layer. A typical interaction layer is shown in Figure 17 and compared to a scheme from Meyer et al. [13]. The interaction layer varied throughout the samples and present different characteristics from the typical one (Figure 17). Various examples are shown in Figure 18. It can be observed that the interaction layer (UZr_2) is sometimes discontinuous, and that oxi-carbides can be found at the interaction layer. When such characteristics were observed, the measurement was started at the incipient point of the Zr phase, excluding the carbides. The obtained values for Zr layer thickness are reported in Table 10.

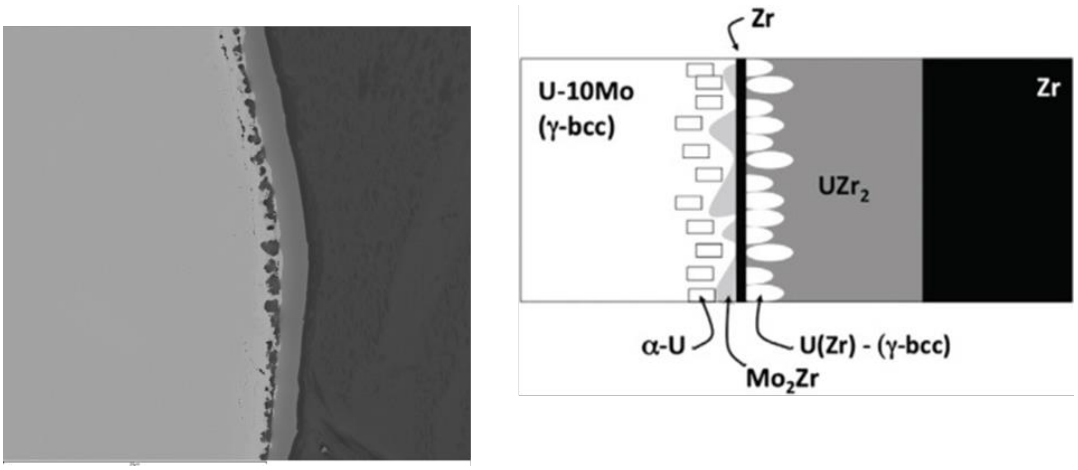

Figure 17. Example of a typical coating observed. The Zr layer observed is compared with the characteristic one shown in Reference[13].

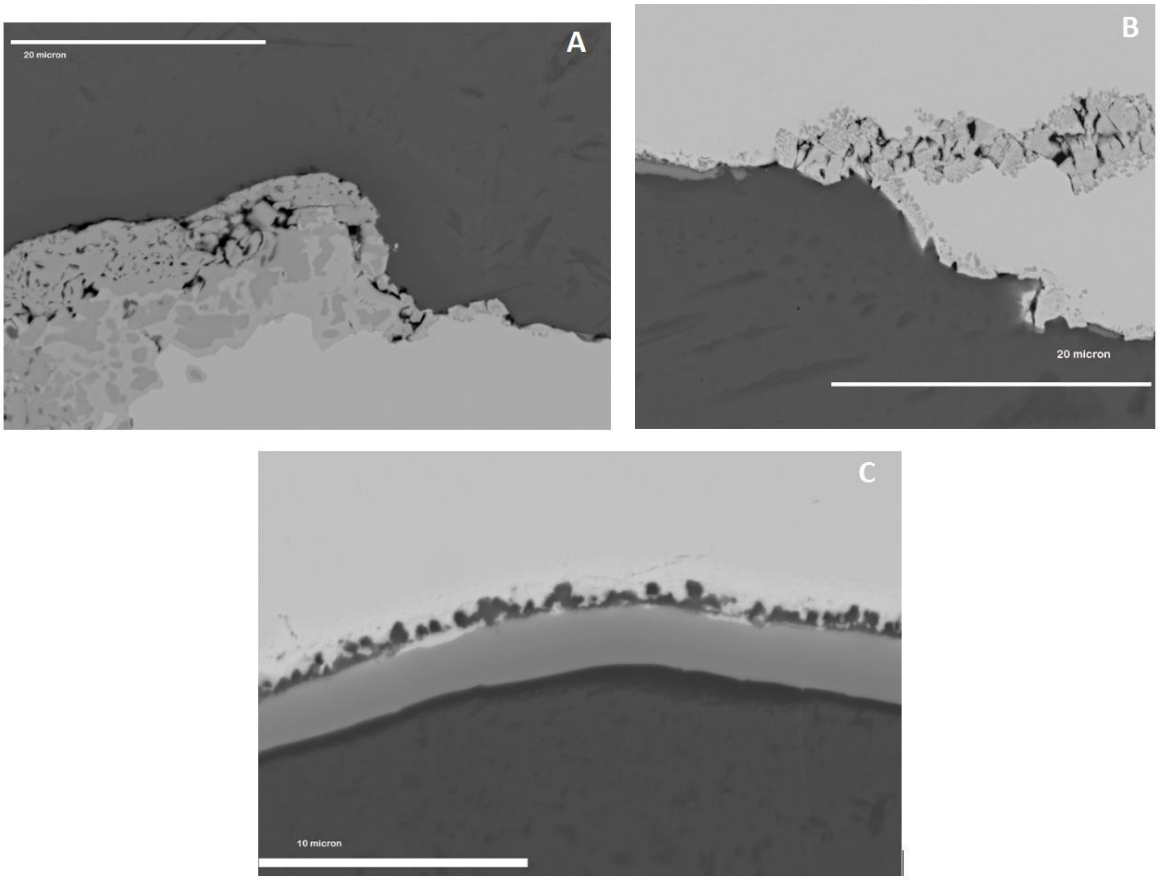

Figure 18. Examples of different Zr interaction layer characteristics: image A and B show the presence of carbides and discontinuity in the UZr_2 interaction layer (029-05-000DTA-Met1-FLongi A, and 029-05-000DTA-Met1-FTrans B); image C shows the characteristic features observed previously (029-05-000DTA-Met2-MLongi).

Table 10. Summary of Zr layer thickness for the foil analyzed. In this table only the sample with a Zr layer are presented. The sample number have been kept in agreement with the previously presented data.

No	Sample Name	Length (µm)	Error (Std σ)	Min/Max (µm)	No	Sample Name	Length (µm)	Error (Std σ)	Min/Max (µm)	No	Sample Name	Length (µm)	Error (Std σ)	Min/Max (µm)
67	029-05-000DTA	56	16	31.7/92.4	91	029-05-0001CTA				115	029-05-006CTB			
68		53	10	35.5/67.9	82					116				
69		56.7	4.3	48.4/67.2	83					117				
70		57	12	19.4/71.9	84					118				
71		59	14	22.4/82.4	95					119				
72		61	12	38.7/77.9	96					120				
73	029-05-002DTB	62	12	34.3/87.5	97	029-05-004CTB				121	029-05-002CTC			
74		49	16	14.6/72.1	98					122				
75		60.2	6.5	48.4/72.1	99					123				
76		55	18	16.4/79.6	100					124				
77		64	10	42/84	101					125				
78		53	15	21.2/81.5	102					126				
79	029-05-000DTC	54	11	21/83.3	103	029-05-1CTC				127	030-01-003CTA			
80		63	11	29.5/75.5	104					128				
81		57.6	6.2	42/65.1	105					129				
82		53	14	18.2/74	106					130				
83		61	13	27.1/83.9	107					131				
84		59	10	39.4/73.7	108					132				
85	030-01-000DTC	109.7	7.8	89.6/129	109	029-05-002CTA				133	030-01-008CTB			
86		131	16	106/159	110					134				
87		114	19	63.7/169	111					135				
88		122	22	54.4/145	112					136				
89		98	16	55.3/123	113					137				
90		90	19	39.9/112	114					138				
										139	030-01-003CTC			
										140				
										141				
										142				
										143				
										144				

The interaction layer was further analyzed by EDX and WDX for elemental composition using line scans and maps and were performed throughout the layer. For each sample, a typical area was chosen for analyses. EDX line scans were taken at HC 15, on a length of more than 10 µm, with a step size of 0.1 µm and an effective count time of 20 s (leading to ~60000 counts for spectra). The line scan was also used to determine the interaction-layer thickness (summarized in Table 11). The WDX/EDX line and full map consisted of 150 frames for the EDX, and 500 frames for WDX, dwell time of 100 s, and current was increased to HC 17. A typical result is shown in the following Figure 19.

Table 11. Thickness measured for the Zr-fuel meat interaction area.

No	Sample Name	Length (µm)	No	Sample Name	Length (µm)	No	Sample	Length (µm)	No	Sample	Length (µm)
67	029-05-000DTA	5.2	91	029-05-0001CTA		115	029-05-006CTB		139	030-01-003CTC	
68		2.0	82			116			140		
69		3.3	83			117			141		
70		3.0	84			118			142		
71		5.0	95			119			143		
72		4.0	96			120			144		
73	029-05-002DTB	3.0	97	029-05-004CTB		121	029-05-002CTC				
74		5.6	98			122					
75		3.6	99			123					
76		3.0	100			124					
77		4.2	101			125					
78		2.6	102			126					
79	029-05-000DTC	4.5	103	029-05-1CTC		127	030-01-003CTA				
80		4.0	104			128					
81		2.7	105			129					
82		3.9	106			130					
83		4.8	107			131					
84		4.3	108			132					
85	030-01-000DTC	4.4	109	029-05-002CTA		133	030-01-008CTB				
86		3.5	110			134					
87		4.6	111			135					
88		6.5	112			136					
89		3.8	113			137					
90		3.5	114			138					

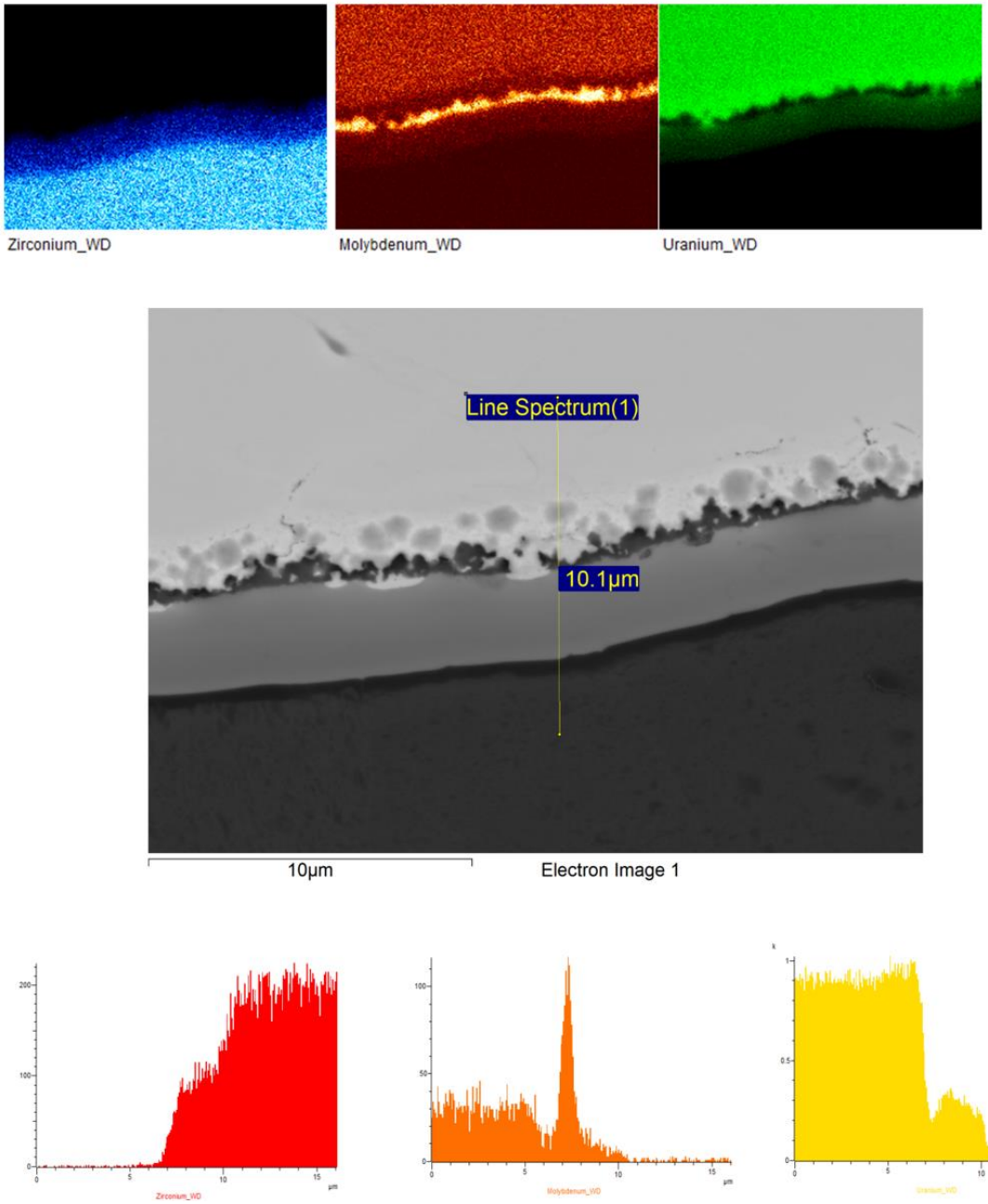

Figure 19. Example of WDX line scan and mapping, showing the interaction layer elemental composition (for Sample 029-05-000DTA-Met3-Longi).

4. DISCUSSION

Most of the analyses in this study were performed following the accorded procedure in References [4,5, and 12]. Some variables have been introduced by utilizing different instrumentation in the laboratory. These differences are highlighted in Table 12, Table 13, and Table 14. From these analyses, it can be inferred that plasma cleaning could improve the optical imaging and SEM analyses, avoiding polishing artifacts observed in some samples. Currently at INL, Aztec software is not available for the JEOL 7600-F; however, an upgrade of the software system is planned in the near future. Due to this, montages are currently performed by coupling low-magnification SEM images with image-analysis software (Photoshop CC2017 [6]). This is also performed for optical images montages.

Table 12. List of the variables introduced during sample preparation.

Sample preparation			
Coating	Polishing	Engraving	Vacuum chamber
Not measured	No Plasma cleaning was used	Adhesive label was used	Not used for met mounts

Table 13. List of the variables introduced during the optical microscope analyses.

Optical Microscope			
Instrument	Montage		Grain Size No.
Zeiss Axo pro 10 mm	BF	2.5, 5, 10 and 50×	30< No. of Grains counted<60
	POL	10, and 20×	

Table 14. List of the variables introduced during the SEM analyses.

SEM/EDX				
	Software	SEM Montage	Elemental Analyses	Thickness
SEM images	Atzec software not available Inca was used	LABE 45-50X with Photoshop In progress	For point analyses ca. 60-80 10^3 counts/point. For EDX mapping ca 6-8 10^6 total counts.	Obtained from SEM image at 45-50 X Zr thickness obtained from 250 X
EDX analyses	Detector	Gamma phase decomposition	Mo distribution/ Chemical Banding	Interaction Layer thickness
	Oxford X-Max 20 mm2	Observed by SEM with LABE detector	Performed on a 70-120 µm line with step 1 µm	Performed on a 10 µm line with step 0.1 µm
WDX analyses	Detector	Elemental composition Interaction layer		
	Oxford Wave Inca	500 frames HC 17		

5. SUMMARY

This report includes the results of the first year's analyses of the MP-1 fuel characterization. During the project limitations of the test plan were recognized, and the test plan was updated and improved. During the first year, all samples have been prepared for analysis, and optical characterization was completed. The most significant limitations included the lack of plasma cleaning, which might improve surface cleanliness, and the lack of an automatic collection features on the optical microscope and SEM, which could significantly decrease data-collection time.

Utilizing the optical microscope, researchers determined the grain size for each of the samples. For most of the samples, similar grain sizes were observed for the different sample sections (forward edge, backward edge, and middle section) analyzed. Some difficulties were highlighted in obtaining the grain size when intense deformation bands were observed. This issue led to a higher standard deviation and larger grain-size diameters for those samples. The grain size is estimated to be approximately 30–40 μm for the cast samples, but 25 μm or smaller for the cold-rolled, annealed samples.

By using the EDX line scan, a reliable evaluation of the Mo distribution could be performed. The average Mo for all samples was between 9.5–10.5%wt. The maximum variation for each sample was, however, lower than the 0.5%wt expected. Due to this problem, researchers were not able to identify chemical banding by imaging with high contrast LABE detector. Some trend for banding may be inferred by the EDX line scan and has been highlighted in the report. They are within the accepted criteria for this working group.

SEM analysis permitted the evaluation of the carbide volume fraction via imaging and, using EDX mapping, a qualitative evaluation of their composition. The carbide volume fraction was estimated using two different ASTM standard methods (both grid manual counting and image analyses with ImageJ software). The volume fraction was less than 1.5% for most samples. The higher carbide fractions obtained were also associated with higher standard deviations and may indicate non-uniform carbide distributions. These images were also analyzed to obtain carbide dimensions. In general, the carbides analyzed contained an area between 3 and 12 μm^2. However, strings of carbides, generally over 200 μm were observed in some samples, may have led to the detection large-area carbides of 1500 μm^2. By EDX mapping of these carbides showed that they include different content of U, C, and O. Oxides and carbides were also observed on the edge of the sample (oxide skins), and these were associated with brittle regions, causing crack formation.

Gamma-phase decomposition may have been observed in some of the samples and was identified by its lamellar feature by SEM. Confirmation of its nature could be obtained by WDX line scan, showing low content of Mo in these regions.

Thickness of the foils and Zr layer were also obtained by the SEM images. The interaction layer was determined by EDX/WDX line scan and map. This showed a large variation throughout the same sample both in terms of composition and thickness and continuity.

6. REFERENCES

1 D. Jadernas, et al., "Microstructural characterization of as-fabricated and irradiated U-Mo fuel using SEM/EBSD" *J. Nucl. Mater.* 509 (2018) pp. .

2 A.J. Clarke, et al., "Microstructural evolution of a uranium-10 wt.% molybdenum alloy for nuclear reactor fuels" *J. Nucl. Mater.* 465 (2015), pp. .

3] B. Beeler, et al., "An atomistic study of grain boundaries and surfaces in γ U-Mo", *J. Nucl. Mater.* Vol. 507 (2018), pp. .

4 Idaho National Laboratory. "Characterization Plan for the Fabrication of U-10 Mo Fuel for the MP-1 Experiment", PLN-5308, Rev.0, 2017.

5 R. Prabhakaran, et al., "U-10Mo Sample Preparation and Examination using Optical and Scanning Electron Microscopy," PNNL-25308, Rev. 1, 2016.

6 T. Knoll et al. "Adobe Photoshop CC," Photoshop 2017.0.1, Version 7, SPI.

7 ASTM-International "Standard Test Methods for Determining Average Grain Size" Designation: E112-13.

8 ASTM-International "Standard Test Method for Determining Volume Fraction by Systematic Manual Point Count" Designation: E562-11.

9 ASTM-International "Standard Practice for Determining Inclusion or Secondary-Phase Constituents Content of Metals by Automatic Image Analyses" E1245-03.

10 *NIH Image to ImageJ: 25 years of image analysis*. Schneider, C. A. and Rasband, W. S. & Eliceiri, K. W. 7, s.l.: Nature methods, 2012, Vol. 9.

11 G.Y. Jeong, et al., "Development of PRIME for irradiation performance analysis of U-Mo/Al dispersion fuel," *J. Nucl. Mater.* 502 (2018), pp. .

12 Idaho National Laboratory, "Characterization Plan for the Fabrication of U-10 Mo Fuel for the MP-1 Experiment," PNNL-5308, Rev.1, 2018.

13 M.K. Meyer et al., "Irradiation performance of U-Mo monolithic Fuel" *Journal of Nuclear Engineering and Technology* 46.2 (April 2014), pp. 169–182.